Controlling influence of water and ice on eruptive style and edifice construction in the Mount Melbourne Volcanic Field (northern Victoria Land, Antarctica)

J. L. Smellie[1]*, S. Rocchi[2] and G. Di Vincenzo[3]

[1]School of Geography, Geology and the Environment, University of Leicester, Leicester, United Kingdom, [2]Dipartimento di Scienze della Terra, Università di Pisa, Pisa, Italy, [3]Istituto di Geoscienze e Georisorse, Consiglio Nazionale delle Ricerche, Pisa, Italy

The Mount Melbourne Volcanic Field (MMVF) is part of the West Antarctic Rift System, one of Earth's largest intra-continental rift zones. It contains numerous small, compositionally diverse (alkali basalt−benmoreite) flank and satellite vents of Late Miocene−Pliocene age (≤12.50 Ma; mainly less than 2.5 Ma). They demonstrate a wide range of morphologies and eruptive mechanisms despite overlapping compositions and elevations, and they occur in a relatively small area surrounding the active Mount Melbourne stratovolcano. The volcanic outcrops fall into several main categories based on eruptive style: scoria cones, tuff cones, megapillow complexes, and shield volcanoes. Using the analysis of lithofacies and appraisal of the internal architectures of the outcrops, we have interpreted the likely eruptive setting for each center and examined the links between the environmental conditions and the resulting volcanic edifice types. Previous investigations assumed a glacial setting for most of the centers but without giving supporting evidence. We demonstrate that the local contemporary environmental conditions exerted a dominant control on the resulting volcanic edifices (i.e., the presence or absence of water, including ice or snow). The scoria cones erupted under dry subaerial conditions. Products of highly explosive hydrovolcanic eruptions are represented by tuff cones. The water involved was mainly glacial (meltwater) but may have been marine in a few examples, based on a comparison of the contrasting internal architectures of tuff cones erupted in confined (glacial) and unconfined (marine, lacustrine) settings. One of the glaciovolcanic tuff cones ceased activity shortly after it began transitioning to a tuya. The megapillow complexes are highly distinctive and have not been previously recognized in glaciovolcanic successions. They are subglacial effusive sequences emplaced as interconnected megapillows, lobes, and thick simple sheet lavas. They are believed to have erupted at moderately high discharge and reduced cooling rates in partially drained englacial vaults under ice, probably several hundred meters in thickness. Finally, several overlapping small shield volcanoes crop out mainly in the Cape Washington peninsula area. They are constructed of previously unrecognized multiple 'a'ā lava-fed deltas, erupted in association with a thin draping ice cover c. 50−145 m thick. Our study highlights how effectively water in all its forms (e.g., snow, ice, and any meltwater) or its absence exerts a fundamental control on eruption dynamics and volcano construction. When linked to published ages and $^{40}Ar/^{39}Ar$ dates produced by this study, the new environmental information indicates that the Late Pliocene−Pleistocene landscape was mainly an icefield rather than a

persistent topography-drowning ice sheet. Ice thicknesses also generally increased toward the present.

1 Introduction

Volcanoes erupt in various environmental settings, including subaerial, subaqueous (lacustrine, marine), and subglacial. Each environment differently influences the erupting magma, resulting in varied eruptive styles and different types of edifices constructed (Cas and Simmons, 2018; Edwards et al., 2022). For example, notwithstanding localized explosivity due to induced fuel–coolant interaction (IFCI) of magmas highly strained during the eruption (Dürig et al., 2020), under deep water conditions, volatile exsolution is largely inhibited, molten fuel–coolant interactions (MFCI) are suppressed, and lava effusion dominates, usually as pillow lava (Kokelaar, 1986; Schmincke and Bednarz, 1990; Clague and Paduan, 2009). At shallower depths, vigorous volatile exsolution and MFCI promote intimate interaction with the surrounding water, resulting in explosive hydrovolcanic eruptions and the generation of abundant lapilli tuffs in tuff cones and tuff rings (Sohn, 1996; White, 1996; Cole et al., 2001; Brand and Clarke, 2009). By contrast, eruptions under fully subaerial conditions, in the absence of surface water or groundwater, are primarily magmatic and construct scoria cones and lava fields (Houghton and Hackett, 1984; Vespermann and Schmincke, 2000). Environmental overburden pressures also directly affect eruptions under ice, known as glaciovolcanic eruptions (Smellie and Edwards, 2016). Thick ice (i.e., high ambient pressures) suppresses explosive

eruptions in favor of lava effusion (pillow lavas), and thin ice promotes the construction of tuff cones (Jones, 1969; 1970; Höskuldsson et al., 2006; Schopka et al., 2006; Pollock et al., 2014). Additionally, because of the buttressing effects of ice, the resulting glaciovolcanic edifices typically have higher aspect ratios (height:basal width) than those formed in unconfined (lacustrine, marine) settings; the latter are much broader and have lower profiles (Smellie, 2013; Pedersen et al., 2020). Thus, the eruptive setting imposed by local environmental conditions can exert a dominating influence on eruption dynamics and edifice construction. Interpreting the eruptive setting can therefore be used as a dipstick to reconstruct past environments and thereby document climate change (Smellie, 2018; Edwards et al., 2022).

We have investigated the flank and satellite centers in the Mount Melbourne Volcanic Field (MMVF), northern Victoria Land, Antarctica (Figure 1) to assess how effective the presence or absence of water has been in determining eruptive styles and edifice construction. Probably because of the glacial environment prevailing today, a glaciovolcanic origin has generally been assumed by previous authors, but supporting evidence has only rarely been presented (cf. Wörner and Viereck, 1987; Wörner and Viereck, 1989; Giordano et al., 2012; Smellie et al., 2018). The centers are mainly small scoria cones but, unusually for volcanism in the West Antarctic Rift System (Smellie, 2021; Wilch et al., 2021), they include several tuff cones, outcrops formed of megapillows and large lava lobes (herein called megapillow complexes), and volcanic shields composed
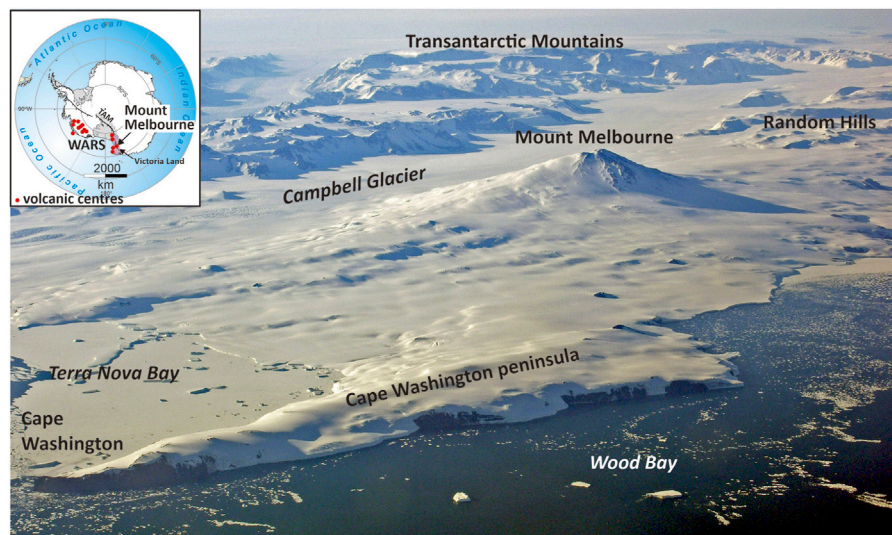
FIGURE 1
Aerial view of the Mount Melbourne Volcanic Field, looking west-northwest. The area is dominated by the prominent symmetrical stratocone of Mount Melbourne. Cape Washington peninsula is formed from several small Late Pliocene coalesced shield volcanoes intruded by Pleistocene strombolian vents. Numerous small centers can be seen as isolated nunataks protruding through the snow at low elevations surrounding Mount Melbourne. The inset shows the location of Mount Melbourne and other large volcanic centers within the West Antarctic Rift System (WARS). TAM—Transantarctic Mountains (stippled). The boundary of the WARS is after LeMasurier (2008).

of multiple lava–breccia couplets (lava-fed deltas), which were previously unrecognized. In this study, the physical volcanology of the centers within the MMVF is described, and the eruptive settings are deduced. Our interpretation of the centers demonstrates that variable local environmental conditions were the dominating control on the eruptive styles and edifices constructed. We show that the variations in eruptive styles and the resulting primary volcanic landforms were overwhelmingly influenced by the presence or absence of water in all its forms (snow, ice, meltwater, and seawater), which, in turn, is linked inextricably to the prevailing climate. Our results are also placed within a comprehensive chronology based mainly on new $^{40}Ar/^{39}Ar$ age determinations. This has enabled a unique view of the terrestrial glacial/interglacial environmental history of the region to be constructed.

2 Geological setting

Antarctica is host to one of Earth's great volcanic rifts, known as the West Antarctic Rift System (WARS) (LeMasurier (2008); Jordan et al., 2020; Siddoway, 2021; Figure 1). Active in stages since the mid-Cretaceous, much of the regional extension probably ceased at c. 26 or possibly 11 Ma, with younger extension focused on the western margin in the Terror Rift and continuing to modern times (Granot and Dyment, 2018; Jordan et al., 2020; Siddoway, 2021). Volcanism has been widespread throughout the WARS. It forms an alkaline association broadly bimodal overall (LeMasurier and Thomson, 1990; Martin et al., 2021; Panter et al., 2021; Rocchi and Smellie, 2021). In Victoria Land, volcanism is contained within the McMurdo Volcanic Group, divided into three large volcanic provinces (Smellie and Martin, 2021; Smellie and Rocchi, 2021). The volcanic edifices throughout Victoria Land consist of (1) polygenetic stratocones characteristic of the inland centers and (2) coalesced shield volcanoes linked to coast-parallel faulting in coastal areas (Hamilton, 1972). There are also numerous small-volume monogenetic centers, mainly scoria cones, scattered over a wide area and known as the Northern Local Suite (Smellie and Rocchi, 2021). The magmatic source for volcanism in northern Victoria Land was initially thought to have originated in an active or fossil mantle plume or a source metasomatized by Palaeozoic subduction. However, the evidence for a mantle plume origin has been strongly criticized (Rocchi et al., 2003; 2005; Rocchi and Smellie, 2021). It is now thought more likely to be related to a combination of (1) generation of an incipient intra-plate boundary between southern Australia and the Ross Sea; (2) craton-directed mantle flow (edge flow) leading to coast-parallel necking and decompression melting; and (3) emplacement of melts along north–south faults and northwest–southeast reactivated Palaeozoic translithospheric transfer faults (Salvini et al., 1997; Storti et al., 2007; Panter et al., 2018; Rocchi and Smellie, 2021).

2.1 Mount Melbourne Volcanic Field

The MMVF is situated in northern Victoria Land. It is part of the Melbourne volcanic province, which contains four other volcanic fields (Smellie and Rocchi, 2021). The MMVF has been described by Wörner and Viereck (1987), Wörner and Viereck (1990), Wörner et al. (1989), Wörner and Orsi (1990), and Giordano et al. (2012) and is summarized here. The petrology is described by Armienti et al.
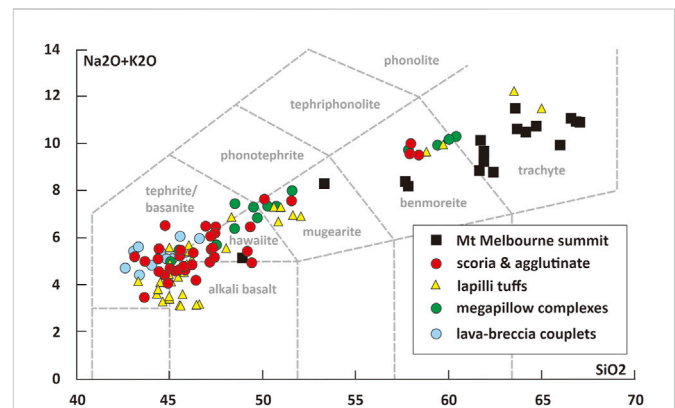

FIGURE 2
TAS diagram (after Le Maitre et al., 2002) for the MMVF showing the wide range of compositions that characterizes the flank and satellite centers and the much more restricted mainly trachytic compositions of volcanic products erupted from the summit of Mount Melbourne. Data from Armienti et al. (1991), Giordano et al. (2012), and unpublished information of the authors.

(1991), Wörner and Viereck (1990), Beccaluva et al. (1991), Lee et al. (2015), and Gambino et al. (2021). Compositionally, the MMVF is a Na-alkaline series, ranging from tephrite/basanite/alkali basalt to trachyte (Figure 2).

Mount Melbourne has a crater or possibly a small caldera 700 m in diameter. The summit is mainly constructed of trachyte to benmoreite domes, scoria and phreatomagmatic cones, and lavas from which the youngest published ages have been obtained (Giordano et al., 2012; Lee et al., 2015). Tephras are also present, including welded fall, and basaltic bombs scattered around the summit attest to recent mafic activity. The crater and upper slope on the north side also contain areas of heated ground and fumaroles (Lyon and Giggenbach, 1974; Lyon, 1986; Wörner et al., 1989; Gambino et al., 2021). The most recent eruption dates back to c. AD 1892–1922 (Lyon, 1986; Wörner et al., 1989), but numerous cryptotephras found in ice cores extend the recent explosive history of Mount Melbourne back to Eemian time, at least 124 ka, possibly 137 ka (Del Carlo et al., 2015; Narcisi and Petit, 2021). Outcrops at lower elevations, which represent flank and satellite vents, are the focus of this study and are scattered widely surrounding Mount Melbourne. They are generally isolated and small, with the largest snow-free outcrops at Edmonson Point and Shield Nunatak. Apart from a small isolated trachyte dome or lava c. 3 km west-northwest of Edmonson Point, the flank and satellite outcrops are tephrite/basanite to benmoreite in composition. They are mainly scoria cones showing variable degrees of degradation, but there are also outcrops of palagonitized lapilli tuffs described as tuff rings, together with enigmatic outcrops composed of megapillows and large lava lobes. Additionally, our study identified several outcrops composed of 'a'ā lava-fed deltas mainly confined to the Cape Washington peninsula (Figure 3).

Radioisotopic ages for rocks in the MMVF are mainly based on K-Ar data (Armstrong, 1978; Wörner et al., 1989; Armienti et al., 1991; Lee et al., 2015), mostly without analytical details. More recently, Giordano et al. (2012) reported $^{40}Ar/^{39}Ar$ data. The previously published results were based on old constants (decay constants and/or the age of the reference mineral) and are therefore
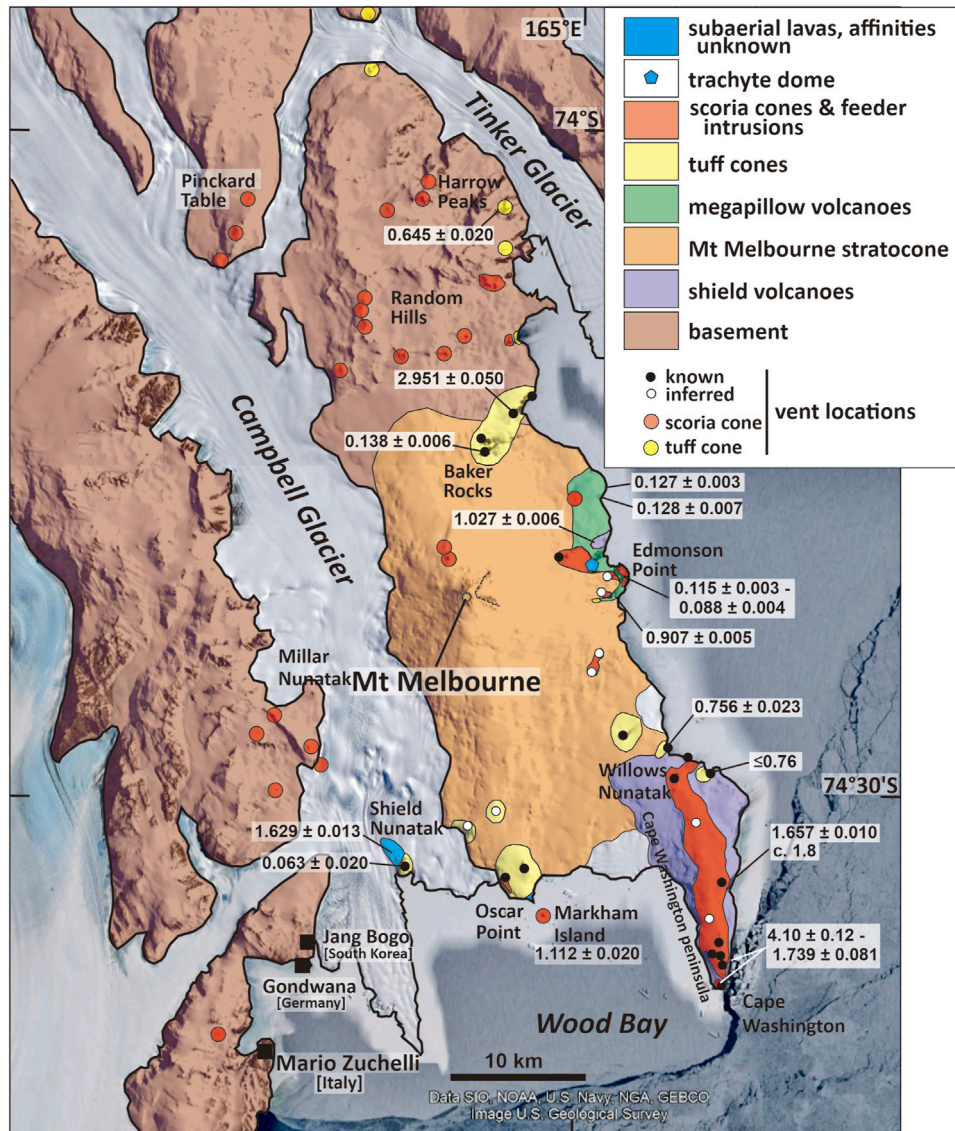
FIGURE 3
Map of the solid geology of the Mount Melbourne Volcanic Field. The sizes of some of the smaller outcrops are exaggerated for clarity. The ^{40}Ar/^{39}Ar ages (Ma) determined by this study are also shown, followed by ± 2σ internal uncertainties. For the locations of other published ages, see Supplementary Figure S1. Several scoria cone and a few of the tuff cone outcrops were not visited during this investigation. Their locations are culled from Wörner et al. (1989) and Armienti et al. (1991) and from our binocular observations.

expected to be c. ≤ 1% younger, but these variations fall largely within the analytical uncertainties. The radioisotopic ages suggest that volcanism began in the Late Miocene (c. 12.5 Ma) but became widespread from the Pliocene (from c. 4 Ma but mainly after c. 2.5 Ma). It continues today, although no eruptions have been witnessed (Wörner et al., 1989; Giordano et al., 2012; Gambino et al., 2021). Units dated by the K-Ar method are mainly intrusions in tuff cones and range in age from 2.96 ± 0.2 to 0.2 ± 0.04 Ma but including an outlier age of 12.50 ± 0.18 Ma (Supplementary Figure S1). ^{40}Ar/^{39}Ar ages published by Giordano et al. (2012) included samples from Edmonson Point, Shield Nunatak, Markham Island, Harrow Peaks, and Random Hills (Figure 3). The dated outcrops vary from scoria cones and associated lava fields to ignimbrite and a lava in one of the megapillow complexes. The localities do not overlap with those dated by K-Ar, and the ages range between

1.368 ± 0.009 and 0.0907 ± 0.019 ka. The 2-σ uncertainties are generally quite high.

3 Methods

Fieldwork occurred in 2005–2006, 2011, and 2014, using helicopter logistics provided by the Programma Nazionale di Recherche in Antartide (PNRA) of Italy. The localities visited are shown in Supplementary Figure S2. A new lithostratigraphic geological map is presented in Figure 3, together with the first detailed geological maps of many outcrops. Rock samples were taken for petrography, radioisotopic dating, and whole-rock analyses. More than 100 thin sections were examined, and 22 samples were analyzed by the ^{40}Ar/^{39}Ar dating method.

TABLE 1 Characteristics of lithofacies in flank and satellite centers of the Mount Melbourne Volcanic Field.

Lithofacies	Characteristics
Sheet lava [sL][a]	Thin sheets and lenses of vesicular finely crystalline 'a'ā lava. Two types of occurrence: (1) small lava fields sourced in scoria cones and (2) shallow-dipping (c. 5°) sequences overlying lava lobe-bearing breccia. In (1), the sequences are up to a few tens of meters thick; the lavas have massive centers c. 0.3–0.5 m thick (rarely up to 20 m) with coarse irregular to columnar joints and grey to red oxidized autobreccias up to 3 m thick (Figure 4B). Also occur as a capping sequence 60 m thick on the tuff cone forming Shield Nunatak; those lavas, probably sourced in a summit scoria cone, transform down-dip into invasive lavas within lapilli tuffs. In (2), the lava sequences vary from 15 to >80 m thick, comprising 2–4 m of massive lava (rarely up to c. 20 m) associated with a similar thickness of autobreccia in which the clinkers are commonly oxidized; the lavas pass down into lava lobe-bearing breccia (lithofacies cB), with which they form cogenetic lava–breccia couplets; the outcrops are mainly confined to Cape Washington peninsula
Compound lava [cL]	Pāhoehoe lava is present at one locality only (4.5 km northwest of Edmonson Point); includes tumuli and entrail pāhoehoe; flow directions suggest derivation from a source upslope to the west, probably the prominent large scoria cone present there, with which there is a compositional match
Pillow lava [pL]	Minor lithofacies; occurs as invasive lava pillows at Baker Rocks (south) between 400 and 600 m asl; the pillows have irregular shapes and are 0.7–3 m across, showing fluidal surfaces and marginal peperite (Figure 4F); stratification is destroyed in adjacent lapilli tuffs; associated with irregular lava tubes 2–6 m thick and up to 50 m long. Pillows also locally developed at margins of invasive lavas intruding lapilli tuffs at Shield Nunatak (Figure 4H)
Megapillows, lobes, and sheets [MpL]	Highly distinctive lithofacies, seen at Edmonson Point (benmoreite to Si-poor trachyte) and to the north, northwest and southwest of Edmonson Point (hawaiite and mugearite); outcrops mostly extend up to c. 200 m asl but highest elevation is c. 400 m asl in nunatak northwest of Edmonson Point; the lava masses are interconnected, comprising irregularly shaped megapillows 4–12 m in diameter, and lobes and sheets a few tens of meters high and a few tens of meters (lobes) to a few hundred meters (sheets) long (Figures 9A–C); rare lava pillows 25–40 cm in diameter (rarely to 1 m) present locally at base of some lava sheets; dark grey aphanitic margins c. 10 cm thick with patchy glassy rinds c. 1–2 cm thick; pale grey and fine grained internally; prominent jointing, of several types (Figure 10; terminology after Lescinsky and Fink, 2000): marginal closely spaced (≤10 cm, down to mm scale) sheeting joints prevalent; they are cross-cut by more widely spaced (c. 20 cm) sheet-like joints, which give way internally to entablature with small prismatic columns (20–50 cm wide; usually <30 cm); entablatures ubiquitous, especially prominent in the lava sheets (Figures 9B,C); some of the larger lava lobes also have basal colonnades developed intermittently, much thinner (few meters) than the overlying entablatures (Figure 9C); the smaller megapillows and rare lava pillows (lithofacies pL) are often radial jointed; blocky joints are well developed where exposed surfaces cut deeply into lobes or megapillows, often accompanied by subordinate pseudopillow joints; joint surfaces occasionally show multiple glassy/aphanitic rinds; some lobes and megapillows show alternating bands of abundant vesicles and non-vesicular lava that are parallel to the lava margins; the vesicles vary from spherical to stretched in an outward direction; the paired bands are up to 2 m thick and pass down into massive non-vesicular lava forming the lava interiors; many lobes and megapillows also have giant ovoid (arched-roof) to spherical vesicles <15 cm in diameter (rarely up to 40 cm); rare irregularly shaped cavities also present, varying from 1 to a few meters in diameter, with fretted glassy internal surfaces (Figure 9D); minor autobreccias present, a few dm to rarely a meter thick, formed of vesicular aphanitic to glassy clinkers 1–10 cm in diameter with strongly stretched vesicles; many clinkers have broken fluidal shapes and often have a weak maroon or rusty brown coloration
Basalt intrusions, irregular and sheet-like [iL]	Pale grey irregular masses and sheets of intrusive basalt occurring in two situations: (1) invading massive to crudely stratified oxidized scoria lapillistones (lithofacies LP), which occur as screens and foundered masses; and (2) within stratified lapilli tuffs (lithofacies LT). Spectacular exposures of (1) are present in the eastern cliffs north of Cape Washington; the basalts are massive to coarsely columnar jointed. In (2), the basalts are spectacularly entablature jointed throughout, sometimes with megapillows developed marginally (Figure 4G); similar intrusive necks, but entablature-jointed, intrude scoria lapillistones at Shield Nunatak and the outcrop east of Willows Nunatak (Figures 6, 7)
Scoria and agglutinate [LP]	Commonest lithofacies in the MMVF. Mainly amorphous piles of scoria; a few have snow-filled craters. The greatest vertical exposure is c. 90 m at Markham Island (Figure 4A). Massive to weakly bedded coarse scoria and broken bombs, including dense cannonball bombs and armored bombs with scoria cores, usually oxidized. Lenses of weakly welded agglutinate up to 15 m thick, with flattened bombs up to 1.7 m and clastogenic lavas
Lapilli tuff, diffusely stratified [dsLT]	Common volcaniclastic lithofacies. Lapilli tuff with prevalent diffuse stratification lacking sag structures below outsize clasts; 1%–2% accessory lava blocks up to 20 cm in diameter; accidental (bedrock-derived) clasts absent but may occur in basal lapilli tuff beds at Harrow Peaks (Giordano et al., 2012). Ash-coated lapilli noted at three localities (Shield Nunatak, northern Baker Rocks, and Harrow Peaks). Outcrops strongly eroded, but craters rarely preserved (at south Baker Rocks, summit of Shield Nunatak, and Oscar Point summit); crater-rim unconformities seen at Baker Rocks (north) and northeast of Baker Rocks. Stratification is disturbed and often destroyed in lapilli tuffs in large areas within outcrops at Shield Nunatak and Harrow Peaks (Smellie et al., 2018). Deformation (slumps, slides) prominent in "Oscar cliff" outcrop (Figure 16)
Lapilli tuffs, well-bedded, graded [glLT]	Minor lithofacies; fine lapilli tuffs forming well-defined beds a few dm to 3 m thick, laterally continuous except where amalgamated (common); reverse-graded bases and normal-graded tops with faint planar laminations; loading structures seen in fine (tuffaceous) tops of beds (Figure 4D)
Coarse tuff, diffusely stratified to dune-bedded [dsT; xT]	Minor lithofacies; very similar to diffusely stratified lapilli tuff lithofacies but thinner stratification and with uncommon steep-faced dune bedforms
Thin-bedded coarse and fine tuffs [bT]	Minor lithofacies; alternating beds 10–15 cm thick with planar and ripple cross laminations
Fine tuff, laminated [glT]	Minor lithofacies; planar laminations, normal grading, amalgamation; rare ripple cross laminations, flame structures, slumping

(Continued on following page)

TABLE 1 (*Continued*) Characteristics of lithofacies in flank and satellite centers of the Mount Melbourne Volcanic Field.

Lithofacies	Characteristics
Hyaloclastite [H]	Minor lithofacies occurring as lenses usually <30 cm thick and a few meters in extent associated with megapillows, lobes and lava sheets at Edmonson Point, with which they are compositionally identical; fines-poor, formed of blocky, glassy to aphanitic lava fragments typically 1–3 cm in diameter (Figure 9E); usually massive but some show laminated coarse sand to granule-grade bases overlain by coarser reverse-graded to normal-graded hyaloclastite; intact and fragmented small lava pillows common
Pumice lapilli tuff [pLT]	Minor lithofacies only found as lenses 1.5–4 m thick and up to 20 m long associated with compositionally identical megapillow, lobes, and lava sheets at Edmonson Point; weakly lithified to unlithified, variably tuffaceous, and full of white to fawn-brown-colored, angular to abraded pumices up to 12 cm in diameter (mainly 1–10 mm) and up to 5%–10% of aphanitic lava clasts; rare small lava pillows (Figure 9F); varies to fine lapillistone; rare faint planar lamination basally, then reverse- to normal-grading above. The Thickest deposit occurs on the high ridge on the inland side of Edmonson Point, overlying megapillow complex; it may be >20 m thick, comprising diffusely stratified fine pumiceous lapilli tuffs with numerous bombs up to 35 cm across, some breadcrusted, others flattened and dense (obsidian-like); the deposit also contains rare thin (<6 cm) lenses of wavy planar laminated tuff
Lava lobe-bearing breccia [cB]	Varies from c. 25 to >115 m thick; always associated with capping ‘a‘ā lava sequences, with which they form cogenetic lava–breccia couplets; the host breccia is massive or rarely crudely homoclinally stratified and formed of coarse aphanitic lava clasts (Figure 9G), generally fines-free or with a minor, patchy coarse or very coarse sand-grade matrix; lava clasts are blocky with planar faces and poorly or non-vesicular; mostly dominated (up to c. 95%) by irregular prismatic and blocky-jointed lava lobes of aphanitic lava up to c. 7 m thick showing closely spaced (1 or 2 dm) irregular joints, blocky joints or entablature with narrow columns (individually typically c. 25 cm wide) that may break up marginally into massive lava breccia; some lobes are partially encased in autobreccia with oxidized clinkers; the breccia in the outcrop north of Edmonson Point is distinguished by two prominent parallel and essentially horizontal orange color bands c. 70 cm thick each, caused by enhanced alteration (Figure 9H)

[a]Lithofacies notations after Smellie and Edwards (2016), slightly modified.

Radioisotopic dating was carried out at the Istituto di Geoscienze e Georisorse, Consiglio Nazionale delle Ricerche (Pisa, Italy). ^{40}Ar/^{39}Ar dates are consistent with the age reported for the reference mineral Fish Canyon sanidine by Kuiper et al. (2008). Full descriptions of the dating results and methods used are presented in Supplementary Figure S3. Elevations and unit thicknesses were determined by hand-held GPS (Garmin eTrex), adjusted for daily pressure drift, and calibrated to fixed locations in the field, with an estimated error of ± 10 m. The terminology for volcaniclastic rocks follows that of White and Houghton (2006), modified to include lapillistones (after Smellie and Edwards, 2016). Additionally, "accessory" and "accidental" refer to cognate lithic clasts and bedrock-derived clasts unrelated to the volcanic center, respectively (Fisher and Schmincke, 1984). Rock compositional names are after Le Maitre et al. (2002).

4 Eruptive styles of flank and satellite centers in the Mount Melbourne Volcanic Field

The volcanic sequences in the MMVF are composed of a comparatively small number of lithofacies and architectures, which together define at least four categories as follows: 1) scoria lapillistones and lava fields, 2) lapilli tuffs and tuffs, 3) megapillow complexes, and 4) lava–breccia couplets. Their principal characteristics and the lithofacies notations used are described in Table 1. Additionally, the trachyte lava or dome present northwest of Edmonson Point (Figure 3) is >180 m thick, multi-colored (pale khaki yellow, green-grey, and cream) with a sugary crystalline texture. It is unconformably overlain by unrelated ‘a‘ā lavas, but it is an isolated occurrence. Its age is unknown (older than 112 ± 84 ka; Supplementary Figure S1). Neither the upper nor lower contacts of the trachyte are exposed, and it is not considered further.

4.1 Scoria lapillistones and lava fields

The scoria deposits form variably degraded pyroclastic cones constructed mainly of massive to crudely bedded fines-free deposits dominated by oxidized scoria (LP; Figure 4A). They are associated with agglutinate, clastogenic lavas, and ‘a‘ā (sL; rarely pāhoehoe [cL]) lava fields (Figure 4B). The lavas have oxidized autobreccias. Additionally, prominent thick, irregular crystalline intrusions with coarse, crude prismatic joints occur at depth in outcrops on the Cape Washington peninsula (iL; Figure 5). The characteristics of the outcrops are indicative of weakly explosive and effusive magmatic eruptions in the absence of groundwater or surface water (or snow/ice).

4.2 Lapilli tuffs and tuffs

At least 12 discrete outcrops formed of lapilli tuff and tuff are present in the MMVF (Figure 3). They are strongly eroded. All the outcrops are dominated by khaki-yellow fine lapilli tuffs with dips often between 18 and 24 but varying to horizontal (Figures 6, 7). Crater-rim unconformities are preserved in strata high in the outcrops at northern Baker Rocks and on the coast northeast of Baker Rocks. Important characteristics include predominant planar, diffuse, discontinuous stratification, rare low-angle cross-stratification, and monomict compositions, with minor accessory lava clasts and scarcity of impact structures beneath outsize clasts (dsLT, dsT). Clasts are blocky and variably vesicular sideromelane and poorly sorted, they often contain abundant fine ash-size matrix, and some contain ash-coated lapilli. These are characteristics shared by deposits formed from dilute pyroclastic density currents (PDCs) during explosive hydrovolcanic eruptions (Branney and Kokelaar, 2002). They result in the construction of tuff cones and tuff rings, but the absence of accidental (bedrock-derived) clasts (except possibly in basal beds at

TABLE 2 Summary of new [40]Ar/[39]Ar ages for volcanic rocks of the Mt Melbourne Volcanic Field[a]

Sample #	PNRA #	Locality	Lithology	Analyzed material	Total gas age (Ma)[b]	±2σ	Plateau age (Ma)[b]	±2σ	[39]Ar(K) % plateau or number of grains in the weighted mean	Preferred age
					Irradiation PAV-66					
T5.5.4	11.12.05JS4	Harrow Peaks	Lava (intrusion in tuff cone)	Groundmass	0.619	0.020	**0.645**	**0.020**	51.4	Plateau
T5.3.4	07.12.05JS4	N of Willows Nun	Lava (intrusion in tuff cone)	Groundmass	0.769	0.025	**0.756**	**0.023**	74.1	Plateau
T5.4.6	09.12.05JS3	Shield Nunatak	Lava	Groundmass	0.064	0.028	**0.063**	**0.020**	95.7	Plateau
T5.17.1	25.12.05JL1	Shield Nunatak	Lava	Groundmass	1.663	0.015	**1.629**	**0.013**	80.9	Plateau
T5.10.2	14.12.05JS2	Markham Island	Lava, clastogenic	Groundmass	1.104	0.026	**1.112**	**0.020**	99.7	Plateau
T5.15.1	20.12.05JA1	Baker Rocks, south	Lava pillow (intrusive; in tuff cone)	Groundmass	0.139	0.009	**0.138**	**0.006**	100.0	Plateau
T5.36.3	09.01.06JS3	NE of Baker Rocks	Lava (intrusion in tuff cone)	Groundmass	2.958	0.055	**2.951**	**0.050**	83.0	Plateau
T5.18.1	25.12.05JL6	7 km north of Edmonson Point	Lava, megapillow	Groundmass	0.127	0.010	**0.1284**	**0.0066**	100.0	Plateau
T5.34.1	08.01.06JS1	Edmonson Point	Lava	Groundmass	0.0984	0.0047	**0.0877**	**0.0043**	70.9	Plateau
T5.34.3	08.01.06JS3	Edmonson Point	Pumice (ignimbrite)	Alkali feldspar	0.1157	0.0029	**0.1147**	**0.0028**	11/11	Plateau
T5.37.3	11.01.06JS3	Cape Washington summit	Lava (juvenile clast in tuff cone)	Groundmass	1.86	0.10	**1.739**	**0.081**	61.6	Plateau
T5.37.5	11.01.06JS5	Cape Washington summit	Lava; local delta #4	Groundmass	2.976	0.037	**2.903**	**0.037**	60.6	Plateau
					Irradiation PAV-87					
T11.1.3	18.11.11JS3	Southern Cape Washington peninsula	Lava; local delta #1	Groundmass	4.21	0.10	**4.10**	**0.12**	43.4	Plateau
T11.1.6	18.11.11JS6	Southern Cape Washington peninsula	Lava; local delta #2	Groundmass	3.71	0.12	**3.271**	**0.039**	52.7	Plateau
T11.4.4	21.11.11JS4	Cape Washington	Lava (intrusion in Strombolian vent)	Groundmass	3.018	0.017	**2.913**	**0.012**	83.5	Plateau
T11.22.2	02.12.11JS8	West flank Cape Washington peninsula	Lava; local delta #4	Groundmass	3.156	0.013	**3.161**	**0.011**	56.6	Plateau
T11.5.2	21.11.11JS6	8 km N of Cape Washington	Lava (intrusion in Strombolian vent)	Groundmass	1.650	0.017	**1.657**	**0.010**	79.9	Plateau
T11.5.3	21.11.11JS7	8 km N of Cape Washington	Lava; from lava lobe-rich breccia of lava-fed delta	Groundmass	1.966	0.016	1.792	0.011	33.5	**~1.8**
T11.6.3	22.11211JS3	E of Willows Nunatak, Cape Washington peninsula	Lava (intrudes scoria lapillistones)	Groundmass	0.892	0.012	No plateau	–	–	**≤ 0.76 Ma**
T11.9.1	24.11.11JS1	3 km NW of Edmonson Pt	Lava; lava-fed delta	Groundmass	1.0260	0.0063	**1.0265**	**0.0059**	73.5	Plateau
T11.23.3	03.12.11JS3	2 km SW of Edmonson Pt	Lava, megapillow	Groundmass	0.9193	0.0052	**0.9071**	**0.0047**	79.7	Plateau
T14.20.1	15.12.14JS1	c. 8 km north of Edmonson Pt	Lava, megapillow	Groundmass	0.1281	0.0035	**0.1274**	**0.0029**	100.0	Plateau

[a]See Supplementary Figure S3 for analytical details and the full dataset.
[b]Preferred ages shown in bold; ages are relative to either the reference material Fish Canyon sanidine [FCs, age 28.201 ± 0.046 Ma (Kuiper et al., 2008)—irradiation PAV-66] or the Alder Creek sanidine [ACs, age 1.1848 ± 0.0012 Ma (Niespolo et al., 2017)—irradiation PAV-87].
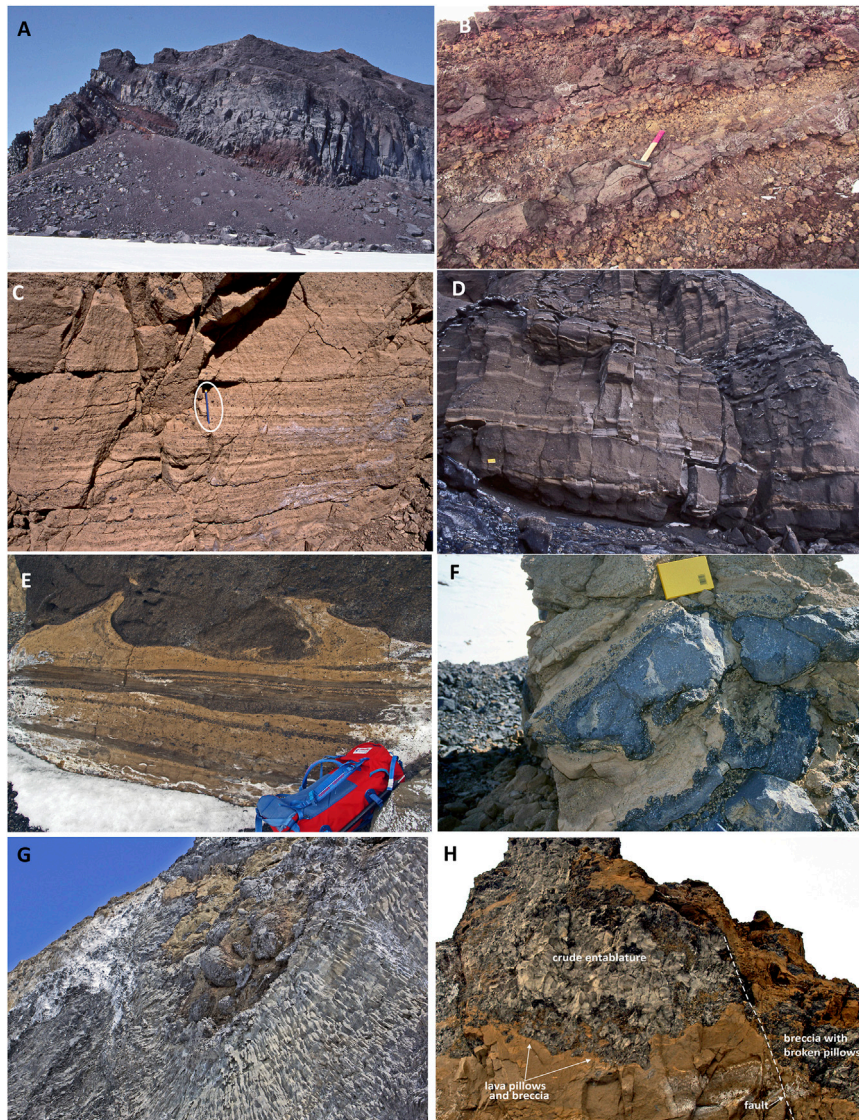
FIGURE 4
Photo compilation showing features of selected lithofacies in scoria and tuff cones in the MMVF. **(A)** View of oxidized scoria, agglutinate, and clastogenic lavas; Markham Island north face; the cliff face is c. 90 m high. **(B)** Close view of 'a'ā lavas and autobreccias; west flank of Cape Washington peninsula, 3.5 km north-northwest of Cape Washington; the hammer is 40 cm long. **(C)** Diffusely stratified fine lapilli tuffs characteristic of the lapilli tuff outcrops; the individual beds are massive, and the bedding surfaces are ill-defined and essentially gradational; Baker Rocks, north; the pencil (ringed) is c. 13 cm long. **(D)** Well-stratified lapilli tuffs and tuffs; the bed surfaces are much better defined than in C; the strata are laterally continuous, often amalgamated, and internally well-structured (normal and reverse grading, planar and wavy lamination, minor soft-state deformation), all features of subaqueous density current deposits (Mulder and Alexander, 2001; Moorhouse and White, 2016); the wavy laminations are probably transitional to ripples; the strata crop out at an elevation of c. 300 m asl; outcrop northeast of Baker Rocks; the notebook is 17 cm long. **(E)** Close view of lapilli tuff beds showing prominent soft-state deformation (load and flame structures) developed in water-saturated tephra; Shield Nunatak; the rucksack is c. 85 cm long. **(F)** Close view of intrusive lava pillows in lapilli tuffs and tuffs; note the fluidal textures on the surface of the basal pillow shown, the development of peperite, and the disturbance of adjacent stratification; Baker Rocks, south; the notebook is 17 cm long. **(G)** Large dyke-like neck within lapilli tuff outcrop; the intrusion is entablature jointed throughout and develops large pillows marginally where they intrude adjacent lapilli tuffs; the lava pillows are 3–5 m in diameter; outcrop c. 2.4 km north-northwest of Willows Nunatak. **(H)** View looking up at invasive lava within massive fine lapilli tuffs in the western cliffs of Shield Nunatak; the lava can be traced to subaerial sheet lavas out of the view beyond the skyline; it develops lava pillows marginally and breaks up into breccia beyond the small-displacement fault seen at right; the breccia on the right may be due to interaction between the invasive lava and wet tephra or brittle breakage linked to the generation of the fault shown; the rock face is c. 20 m high.

Harrow Peaks; Giordano et al., 2012) is more typical of tuff cones, with the loci of explosions high in the eruptive pile rather than in bedrock. Bedrock-sourced explosions, typically resulting in a high proportion of bedrock clasts (>10 vol%; Sohn, 1996; Ort et al., 2018; Latutrie and Ross, 2020), result in the construction of tuff rings and maars, whereas tuff cones typically form where magma interacts with shallow surface water (lakes or the sea), although they can also form above free-flowing readily recharged aquifers (Sohn and Chough, 1992). The absence of basal pillow lava mounds and pillow lava fragments as clasts in the outcrops indicates that volatile exsolution and explosivity were not suppressed at the outset consistent with low ambient pressures and thus relatively shallow water depths, or possibly relatively thin

FIGURE 5
View of the east side of Cape Washington showing a sequence of 'a'ā lava-fed deltas intruded by intrusive necks and sheets associated with coeval oxidized Strombolian scoria deposits (see also Figure 11). The fine dashed lines indicate the approximate positions of passage zones (subaqueous−subaerial transitions) associated with each lava-fed delta. The locations and ^{40}Ar/^{39}Ar ages (Ma) of dated samples are also shown, with ± 2σ internal uncertainties. The cliff is c. 250 m high.
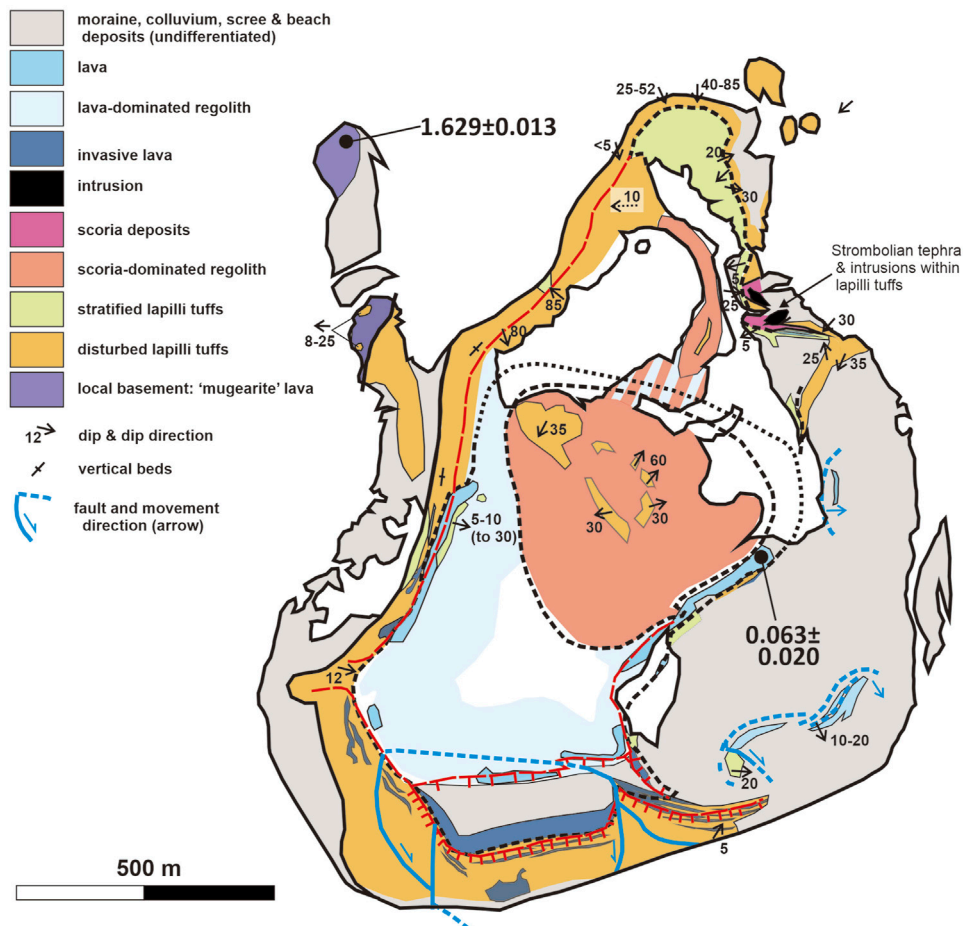

FIGURE 6
Geological map of Shield Nunatak. The locations and ^{40}Ar/^{39}Ar ages (Ma) of dated samples are also shown, with ± 2σ internal uncertainties. Note (1) the often gently inward-dipping upper lapilli tuff strata and (2) the occurrence of scoria lapillistone deposits at two levels (at the summit and within lapilli tuffs in the northeastern cliff face; the latter outcrop also includes entablature-jointed intrusions). Both are features consistent with the eruption in an ice-confined glacial vault involving variable water levels and multiple vents. Very similar relationships also occur in the outcrop east of Willows Nunatak (Figure 7).
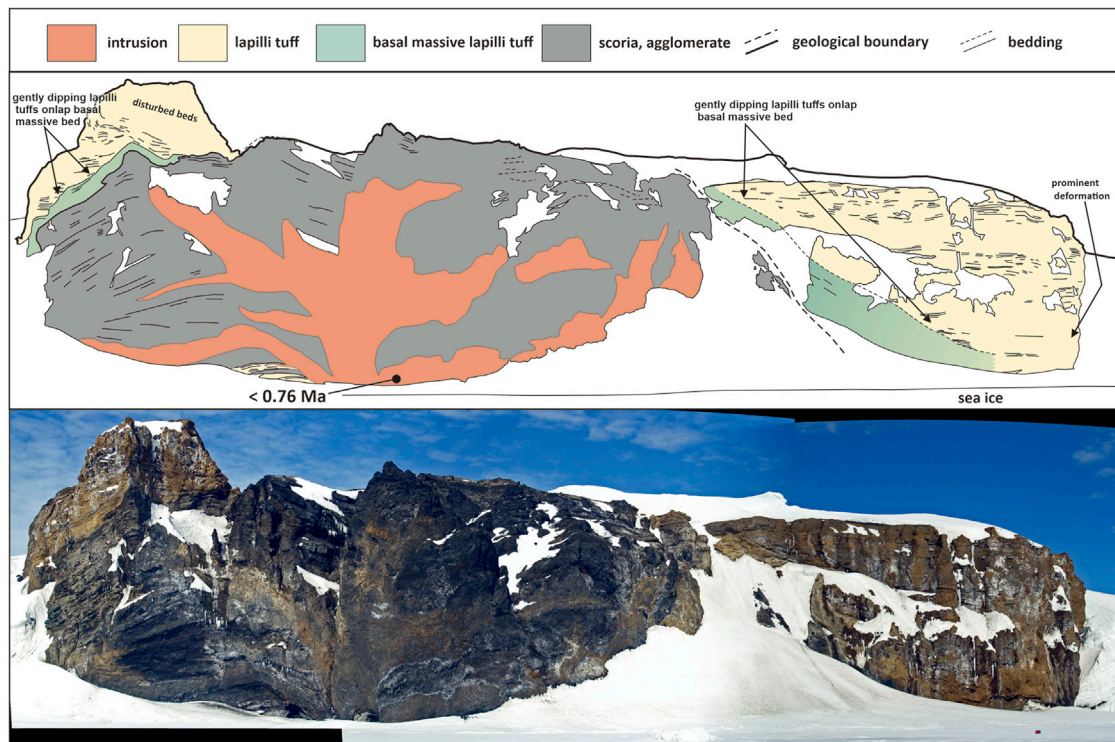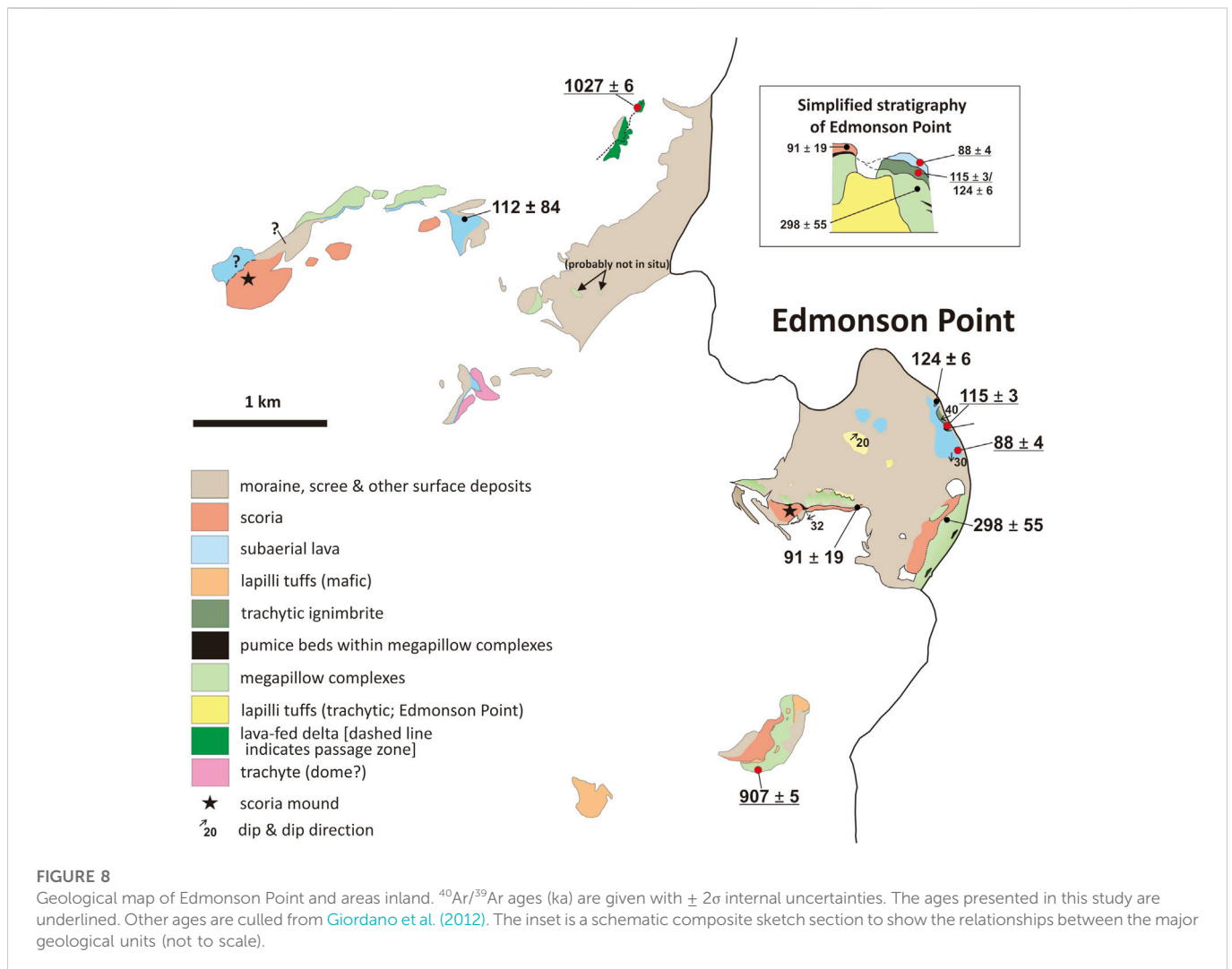
FIGURE 7
Sketch of outcrop east of Willows Nunatak showing the principal lithofacies present. The location and ^{40}Ar/^{39}Ar age (Ma) of the dated sample are also shown, with ± 2σ internal uncertainty. Note the very low dips of the upper (lapilli tuff) strata, consistent with banking against surrounding high ice walls and eruption in a glacially confined vault. Although the central intrusion invades scoria lapillistones, it is pervasively entablature-jointed with blocky and pseudopillow joints, suggesting that the scoria deposit was water saturated by the time the neck was emplaced. Note also the thin lapilli tuff units formed from hydrovolcanic eruptions at the base of the scoria deposits, left of the intrusive neck. The outcrop is petrologically similar throughout (basanite) and was constructed from products of more than one vent, with later vent-clearing hydrovolcanic explosive eruptions forming the massive deposit (green color) that drapes the slightly earlier scoria unit. An eruptive history involving variable water levels and multiple vents is indicated as also occurred at Shield Nunatak, but the outcrop lacks the thin capping sequence of subaerial lavas present at Shield Nunatak (cf. Figure 6). The cliff is c. 100 m high.

overlying ice. Although it is thought that powerful explosive MFCI hydrovolcanic eruptions are increasingly unlikely at water depths exceeding 100 m (Zimanowski and Büttner, 2003; Dürig et al., 2020), the depth of the effusive to explosive transition for mafic magmas is not well defined. Estimates typically range between 100 and 200 m (Jones, 1970; Allen, 1980; White et al., 2003; Schopka et al., 2006; Valentine et al., 2014). Explosivity at greater depths is theoretically possible but probably requires special circumstances (IFCI: Dürig et al., 2020), and the relatively high hydraulic pressures at depths greater than 100–200 m seem likely to severely restrict explosivity (cf. Wohletz, 2003; Chadwick et al., 2008; Resing et al., 2011).

The pervasive diffuse stratification of the dominant lapilli tuff lithofacies, with its ill-defined bedding surfaces (Figure 4C), indicates rapid deposition from PDCs during vertical aggradation of the eruption-fed tephra piles, probably accompanying a sustained continuous-uprush style of explosive activity (White, 2000; Smellie, 2001). The deposits are not diagnostic of depositional settings, which can be subaerial or subaqueous (Sohn et al., 2008; Russell et al., 2013; Sohn and Sohn, 2019). However, the preservation of ash-coated lapilli (sensu Brown et al., 2012) is unlikely if the lapilli fell into and sank through water. They occur in outcrops at northern Baker Rocks, Oscar cliff, Shield Nunatak, and east of Willows Nunatak. In each case, they are confined to the uppermost strata, consistent with subaerial

exposure of the tuff cone in its final eruptive stages. In a few examples, the final eruptive activity consisted of scoria cones, signifying "dry" subaerial conditions [Baker Rocks (south), Shield Nunatak]. Uncommon occurrences of ash-coated lapilli at lower elevations (e.g., at Oscar cliff) might be reworked during discrete mass flow events in which the lapilli were transported while isolated from the overlying water by relatively concentrated PDCs rich in fine tuff. However, tuff cone eruptions within a water-flooded vent occur through repeated ejection and recycling of water-saturated slurries (Kokelaar, 1983). It is an environment that will probably reduce the formation of ash-coated particles and ash aggregates because of the lack of surface tension effects (Go et al., 2017). Ash-coated particles and aggregates are common in the subaerially constructed summit cones formed after the vent is no longer flooded (Sohn et al., 2008).

By contrast, the associated, less common lithofacies may have been deposited mainly under subaqueous conditions. They include lithofacies glLT, dsT, xT, bT and glT (Table 1). They consist of well-structured laterally continuous beds with sharp surfaces and a variety of structures, including amalgamation, reverse- and normal-grading, syn-sedimentary instability (flame structures, soft-state deformation), ripple bedforms, and planar and wavy laminations (Figures 4D,E), which collectively probably indicate subaqueous transport and deposition. Beds of lapilli tuff with well-defined (rather than diffuse) bedding surfaces have been interpreted as

FIGURE 8
Geological map of Edmonson Point and areas inland. ^{40}Ar/^{39}Ar ages (ka) are given with ± 2σ internal uncertainties. The ages presented in this study are underlined. Other ages are culled from Giordano et al. (2012). The inset is a schematic composite sketch section to show the relationships between the major geological units (not to scale).

products of intermittent jetting activity in Surtseyan tuff cones resulting in discrete pulses of tephra cascading down the subaqueous flanks as gravity flows (White, 1996; White, 2000; Smellie, 2001; Sohn et al., 2008). Although there is a resemblance to subaerial deposits (e.g., Sohn and Chough, 1992; Sohn, 1996; Solgevik et al., 2007), it is unlikely that fast-moving subaerial pyroclastic density currents are capable of creating the deposits with (admittedly rare) small (<c. 5 cm amplitude) ripples with steep lee faces, whereas they are a common bedform in subaqueous sequences (Skilling, 1994; White, 1996; White, 2000; Sohn et al., 2008; Moorhouse and White, 2016; Sohn and Sohn, 2019). The soft-state deformation is also more likely to occur in a water-saturated substrate. The absence of steep-sided erosion surfaces, such as incised rills and other channels cut by surface wash, and the absence of ash-coated lapilli are also indirect evidence for a subaqueous depositional setting (Sohn et al., 2008). Additional support is provided by the presence of intrusions at high elevations in the tephra piles showing pervasive entablature or closely spaced irregular jointing and intrusive lava pillows (iL; Figure 4F). The style of jointing and development of lava pillows indicates a water-rich environment. Hence, the tephra piles were water-saturated and presumably surrounded by a lake. Entablature jointing in the coeval intrusions typically extends up to c. 200 m above sea level (asl) but may exceed 300 m asl in the outcrop

northeast of Baker Rocks. The neck or large dyke in the outcrop north of Willows Nunatak also includes marginal megapillows invading adjacent lapilli tuffs (Figure 4G). Finally, the tuff cone outcrop at Shield Nunatak has a capping unit of sheet-like 'a'ā lavas. In part, they are coarsely jointed and finely crystalline consistent with subaerial emplacement, although lacking oxidation of the autobreccias. They were probably sourced from the small summit scoria cone present (Figure 6). However, the lavas transform down-dip into invasive sheets showing the development of aphanitic breccias and pillows (Figure 4H), indicating intrusion into the tephra deposits, which were water saturated and unlithified, and a high coeval water level. Scoria deposits also occur in other lapilli tuff outcrops in the MMVF [east of Willows Nunatak (Figure 7), Baker Rocks (south)]. In summary, the tuff cone outcrops show evidence for subaqueous and subaerial eruptions consistent with an origin as Surtseyan (subaqueous to emergent) tuff cone edifices.

4.3 Megapillow complexes

Outcrops composed of interconnected megapillows, lobes, and lava sheets (MpL) are restricted to the east side of the Mount Melbourne peninsula, at Edmonson Point, and in surrounding
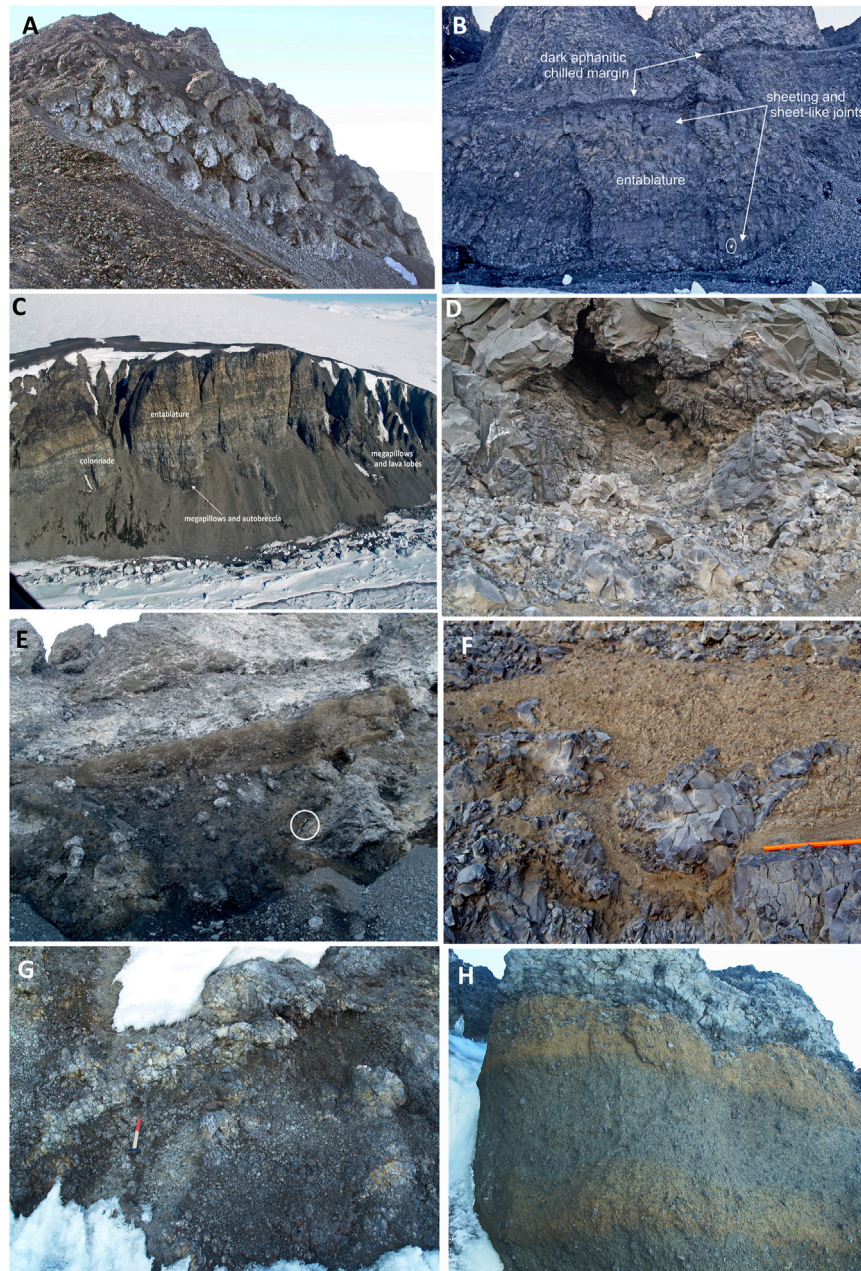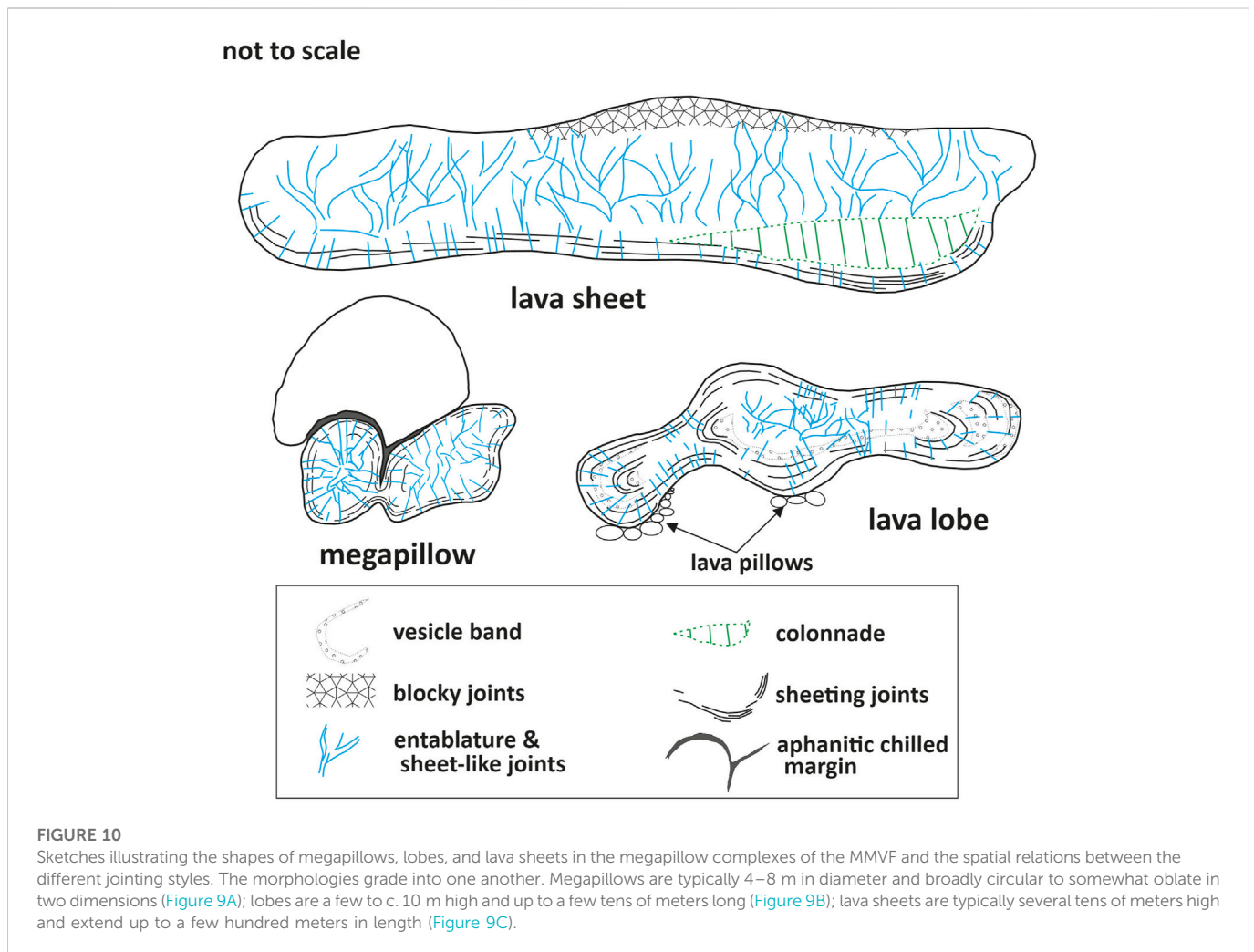
FIGURE 9
Photo compilation showing features of selected lithofacies in the MMVF: megapillow complexes and lava-fed deltas. **(A)** Cluster of close-packed megapillows; the megapillows in this group are unusually well defined; individual megapillows are 4−8 m in diameter; southern Edmonson Point. **(B)** Lava lobe or small sheet 7 km north of Edmonson Point; the lobe is dominated by pervasive closely spaced cooling joints, mainly marginal sheeting joints and prominent central entablature. Sheet-like joints cut perpendicularly across the marginal sheeting joints; the notebook (ringed) is 17 cm long. **(C)** Large lava sheet >500 m long with a thin basal colonnade (pale grey) and overlying much thicker entablature (brown); the lava changes to megapillows and lobes to the right and below; outcrop 7 km north of Edmonson Point; the cliff is c. 200 m high. **(D)** Large void c. 1 m in diameter with fretted glassy surface situated between megapillows, interpreted as a likely ice-block melt-out cavity; southern Edmonson Point. **(E)** Unusually thick lens of massive fine hyaloclastite with dispersed intact and fragmented lava pillows between lava masses; southern Edmonson Point; the ice axe (ringed) is c. 70 cm long. **(F)** Lens of trachytic pumice lapillistone with lava pillows; the pumice deposit shows planar laminations to base; southern Edmonson Point; the pencil shown is 13 cm in length. **(G)** Massive breccia formed of angular, blocky, monomict, aphanitic lava fragments with numerous closely jointed, irregular, water-cooled lava lobes; lava-fed delta outcrop c. 9 km north of Cape Washington; the hammer is 40 cm in length. **(H)** View of lava-fed delta passage zone in the outcrop c. 3.5 km north-northwest of Edmonson Point; the closely jointed lava at the top of the outcrop is water cooled and invades the underlying monomict lava breccia; the breccia also shows two prominent pervasive orange-stained alteration zones, each c. 70 cm thick, interpreted as possible alteration fronts caused by at least two water levels coeval with emplacement of the delta.

nunataks (Figures 3, 8, 9A–C). The division into several morphologies is based on size (terminology after Goto and McPhie, 2004). However, the exposure is only in two dimensions, so the full three-dimensional morphologies of the lava bodies are unknown. Although megapillow shapes can reasonably be inferred for some outcrops (Figure 9A), other megapillows might be cross-sections through tubes. All lava

FIGURE 10
Sketches illustrating the shapes of megapillows, lobes, and lava sheets in the megapillow complexes of the MMVF and the spatial relations between the different jointing styles. The morphologies grade into one another. Megapillows are typically 4−8 m in diameter and broadly circular to somewhat oblate in two dimensions (Figure 9A); lobes are a few to c. 10 m high and up to a few tens of meters long (Figure 9B); lava sheets are typically several tens of meters high and extend up to a few hundred meters in length (Figure 9C).

masses are characterized by multiple sets of prominent cooling fractures, including sheeting, entablature, sheet-like, blocky, and pseudopillow (Figures 9B,C). Blocky joints (also called cube joints or hackly joints) are a more densely fractured version of entablature caused by interaction with larger amounts of coolant and a faster cooling rate (Forbes et al., 2014). The spatial development of the joint types is the same in each outcrop and is concentric to the lava morphology (Figure 10). All the joints are extensional structures, and the style of fracturing and fracture spacing reflect (1) the position of the fractures relative to the lava margins and (2) the cooling history of the lava, that is, progressive inward cooling (Lescinsky and Fink, 2000). They are caused by the rapid chilling of lava against water or ice, and the fracture spacing is inversely proportional to the cooling rate (Long and Wood, 1986; Grossenbacher and McDuffie, 1995; Lescinsky and Fink, 2000; Goehring and Morris, 2008). The marginal sheeting joints wrap around and mimic the shape of the individual lava bodies. They form after the lava has substantially crystallized and are thought to be related to late-stage shear within the lava (Bonnichsen and Kauffmann, 1987). In the absence of exposed surfaces, they are often the best indicator of the overall morphology of the individual lava masses. Moreover, observations of the sheeting joint orientations have shown that most of the lava masses in the MMVF outcrops are probably interconnected. The multiple bands of vesicles observed in some megapillows and lobes are vesicle zones characteristic of

lava inflation (Self et al., 1996; Self et al., 1998). The autobreccia clinkers are also vesicular. Together with the vesicle zones, the features suggest that the lavas were not fully degassed when they erupted.

Lava pillows and megapillows are thought to characterize subaqueous lava emplacement (Batiza and White, 2000; Goto and McPhie, 2004; Hungerford et al., 2014). In the megapillow complexes of the MMVF, the presence of lava pillows and megapillows with glassy rims and lenses of hyaloclastite indicates rapid water chilling. Moreover, entablatures and pseudopillow fractures form by steam and water penetrating down extensional fractures (Long and Wood, 1986; Lescinsky and Fink, 2000; Forbes et al., 2012; Forbes et al., 2014). However, the lava masses typically have dm-thick dark grey rims that are aphanitic or hypohyaline (Figure 9B), and glassy (holohyaline) rims are poorly developed in general. The presence of relatively thin colonnades below some of the lava sheets (Figure 9C) also indicates slow conductive cooling. The observations are inconsistent with the rapid cooling of subaqueous lavas. The sedimentary features of the interbedded lenses of pumiceous lapilli tuff (pLT; Table 1) indicate transport and deposition by tractional and density currents (planar lamination and variable grading; *cf.* Mulder and Alexander, 2001). The abundant highly vesicular pumice is likely to float, suggesting that transport was fluvial unless the pumice was hot when it fell onto the water and ingested water, causing it to rapidly become waterlogged and to sink (Witham and Sparks, 1986). The abrasion observed in
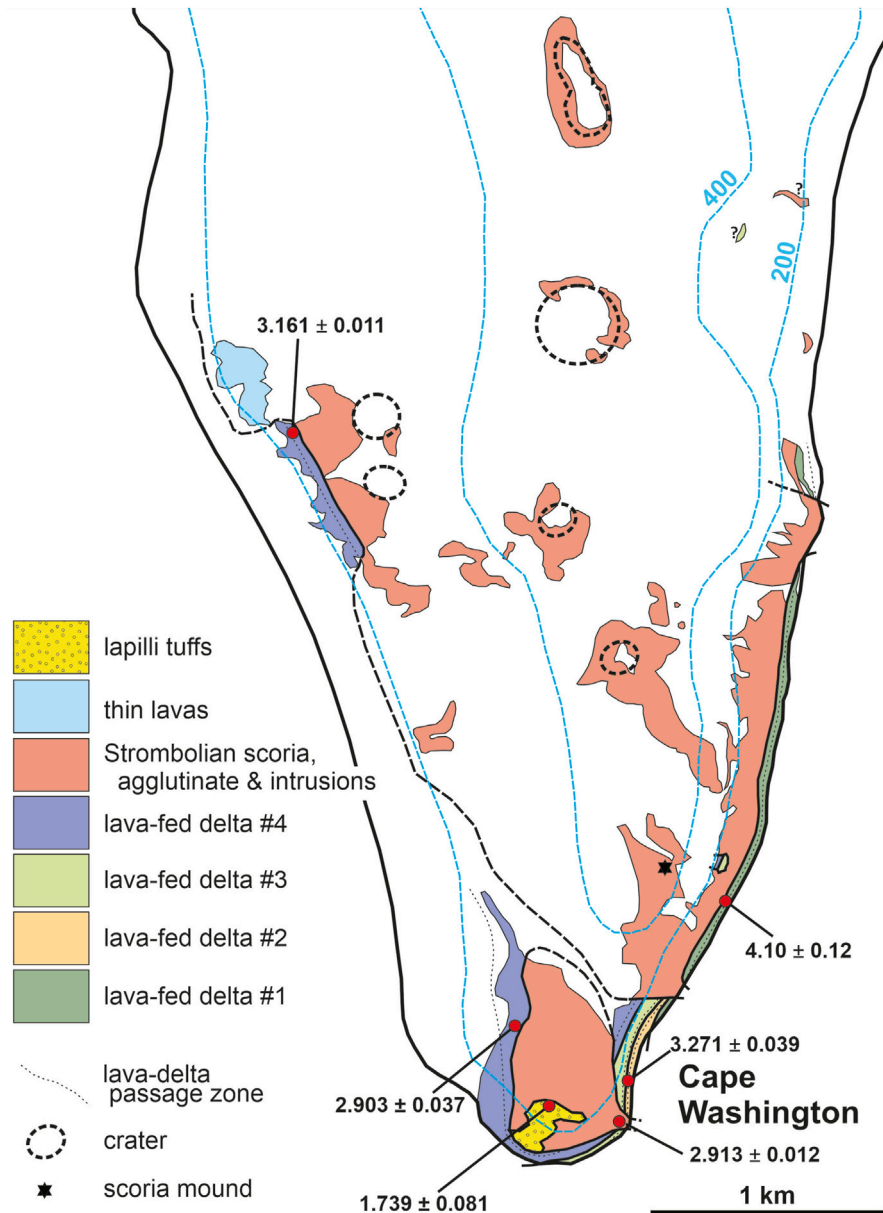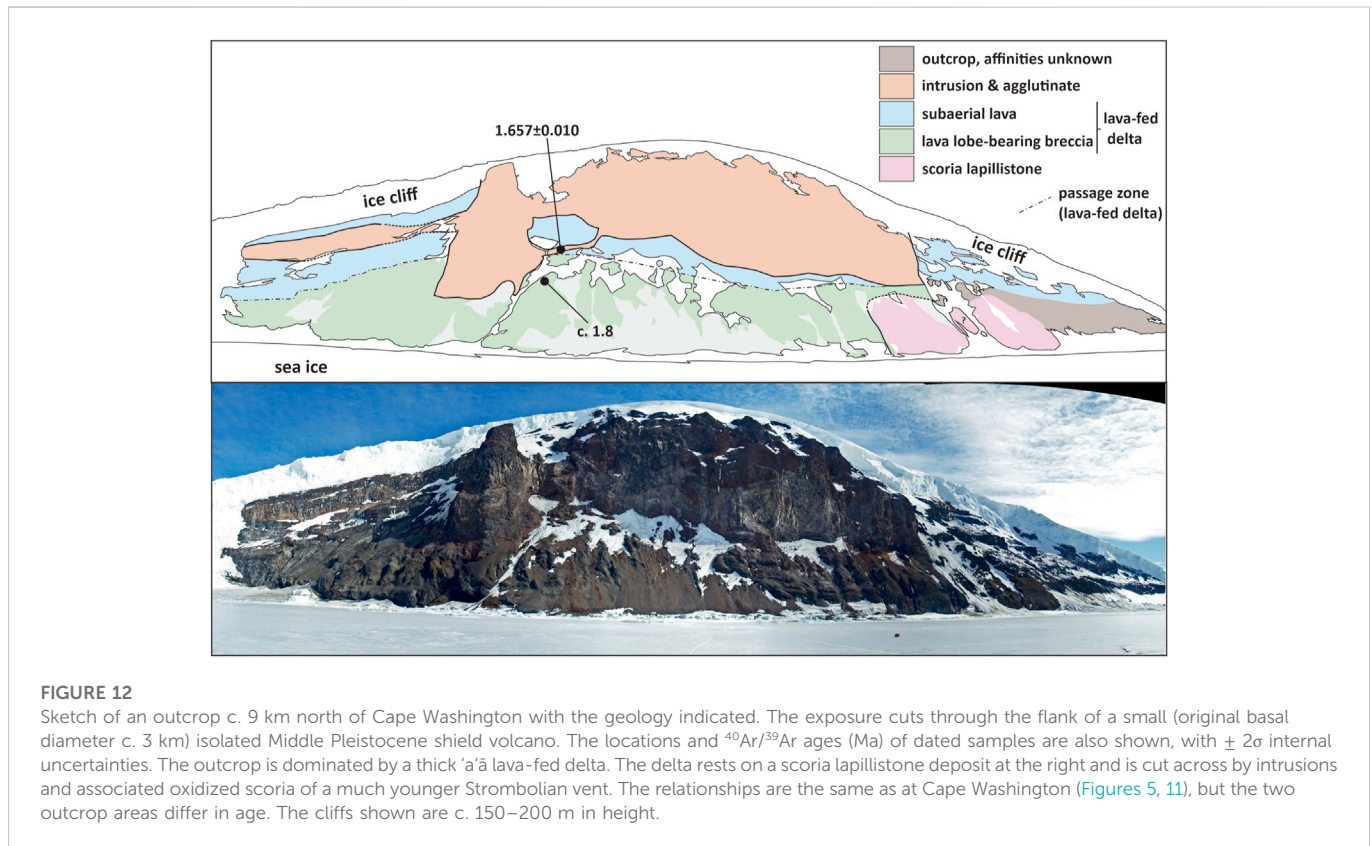
FIGURE 11
Geological map of the southern Cape Washington peninsula, consisting of Pliocene 'a'ā lava-fed deltas cut across by several Strombolian vents. The latter were aligned in a north–south direction and were probably fault-controlled. They comprise prominent tephrite/basanite intrusions that constructed multiple scoria cones formed of oxidized scoria and at least one fed a small field of 'a'ā lava. The locations and ^{40}Ar/^{39}Ar ages (Ma) of dated samples are also shown, with $\pm$ 2σ internal uncertainties. See also Figure 5.

many of the pumices is also consistent with fluvial transport. The aphanitic lava fragments forming the autobreccias, with their fluidal and planar broken faces, resemble the broken crusts seen in many pāhoehoe lavas, but the absence of oxidation suggests that emplacement was not subaerial (i.e., "dry" conditions; Self et al., 1996; Bondre et al., 2004). Thus, the evidence suggests that although water cooling played a prominent part in the emplacement of the megapillow complexes, the individual lava masses may not have been fully submerged (see Section 6.1.3).

Subaqueous lavas are typically categorized on the basis of their morphology as pillowed, lobate, or lava sheets (e.g., Fox et al., 1987; Schmincke and Bednarz, 1990; Gregg and Fink, 1995; Batiza and

White, 2000; Goto and McPhie, 2004; Clague and Paduan, 2009; Hungerford et al., 2014). The distinction is based principally on size, although the lavas also become more flattened as they become larger, and, as described above, they display regular cooling joint patterns (Figure 10; Lescinsky and Fink, 2000). The morphological differences have been related to composition, eruption temperature, cooling rate, effusion rate, viscosity, and crystallinity (Schmincke and Bednarz, 1990; Griffiths and Fink, 1992; Gregg and Fink, 1995, and references therein). However, analog models and studies of ocean-floor lavas have demonstrated that the principal link is to discharge rate and bedrock gradient (Gregg and Fink, 1995; Batiza and White, 2000; Clague and Paduan, 2009). Although pillow

FIGURE 12
Sketch of an outcrop c. 9 km north of Cape Washington with the geology indicated. The exposure cuts through the flank of a small (original basal diameter c. 3 km) isolated Middle Pleistocene shield volcano. The locations and $^{40}Ar/^{39}Ar$ ages (Ma) of dated samples are also shown, with ± 2σ internal uncertainties. The outcrop is dominated by a thick 'a'ā lava-fed delta. The delta rests on a scoria lapillistone deposit at the right and is cut across by intrusions and associated oxidized scoria of a much younger Strombolian vent. The relationships are the same as at Cape Washington (Figures 5, 11), but the two outcrop areas differ in age. The cliffs shown are c. 150−200 m in height.

diameter is known to increase in more evolved magmas (Walker, 1992), studies have shown that a wide spectrum of flow morphologies (i.e., pillow lavas to lava sheets) can occur with negligible compositional differences (Batiza et al., 1989; Batiza and White, 2000) and the rheological effects of composition, temperature, viscosity, and crystallinity are interlinked. There is no compositional dependence evident in the MMVF. Despite the wide range of compositions present in the megapillow complexes (alkali basalt to Si-poor trachyte; Figure 2), similar lava morphologies occur in each outcrop. Moreover, in some (e.g., outcrop 7 km north of Edmonson Point), the lava masses increase in size up through the lava pile despite no obvious compositional variation. Thus, we suggest that the progression of morphologies, from rare pillows through megapillows and lobes to lava sheets, probably reflects increasing discharge rates, with the generally large dimensions due to relatively slow cooling. We suggest that the slower cooling was due to only partial submergence in water; pillow lavas emplaced fully submerged are faster-cooled and, therefore, smaller. Bedrock gradient might have been a contributing factor affecting flow rate, but the observed variations in morphology, which are usually random in the outcrops, would require that the bedrock gradient varied during the course of the individual effusive eruption, which is unlikely unless the lava piled up around the vent, thus increasing the surface gradient over time. Therefore, we suggest that increasing discharge rates at the vent and environmentally imposed slower cooling rates were the likely dominant factors that led to the different lava morphologies in the megapillow complexes. The lowest effusion rates and highest cooling rates were probably responsible for the pillow lavas, the highest effusion rates and slower cooling led to the

lava sheets, and intermediate rates were responsible for the megapillows and lava lobes.

4.4 Lava−breccia couplets

A discovery of the present study was the recognition of multiple lava−breccia couplets within the MMVF. They crop out mainly on the Cape Washington peninsula, particularly close to Cape Washington (Figure 11), but there is an additional small isolated outcrop a few kilometers north of Edmonson Point (Figure 3). The combination of massive chaotic aphanitic lava breccia with abundant irregular lava lobes (cB) capped by subaerially emplaced 'a'ā lavas (sL) is diagnostic of 'a'ā lava-fed deltas (Smellie et al., 2011a; Smellie et al., 2013). The lava-fed deltas have shallow dips of c. 5 consistent with original shield-like landforms. The bedding attitudes of additional outcrops with deltas on the east side of the Cape Washington peninsula indicate that multiple small shield-like volcanoes are present (Figure 12). The upper surfaces of only two lava-fed deltas (#1 and #3) were accessible. They are erosive (Figure 13), resulting in the capping 'a'ā lava sequences of both deltas thinning markedly in a southerly direction. The thickest sequence (c. 250 m) is at Cape Washington and comprises four superimposed lava-fed deltas (Figures 5, 11). The lava lobes in the breccia lithosomes show strong evidence for water chilling in the form of diagnostic joint patterns (mainly closely spaced, irregular, or blocky), and the lobes often break up marginally into aphanitic lava breccia. Oxidized clinkers are also dispersed in the breccias and partially encase lava lobes, which are distinctive features of water-chilled lavas and breccias in 'a'ā lava-fed deltas (Smellie et al., 2013). The number of lava lobes increases up toward the
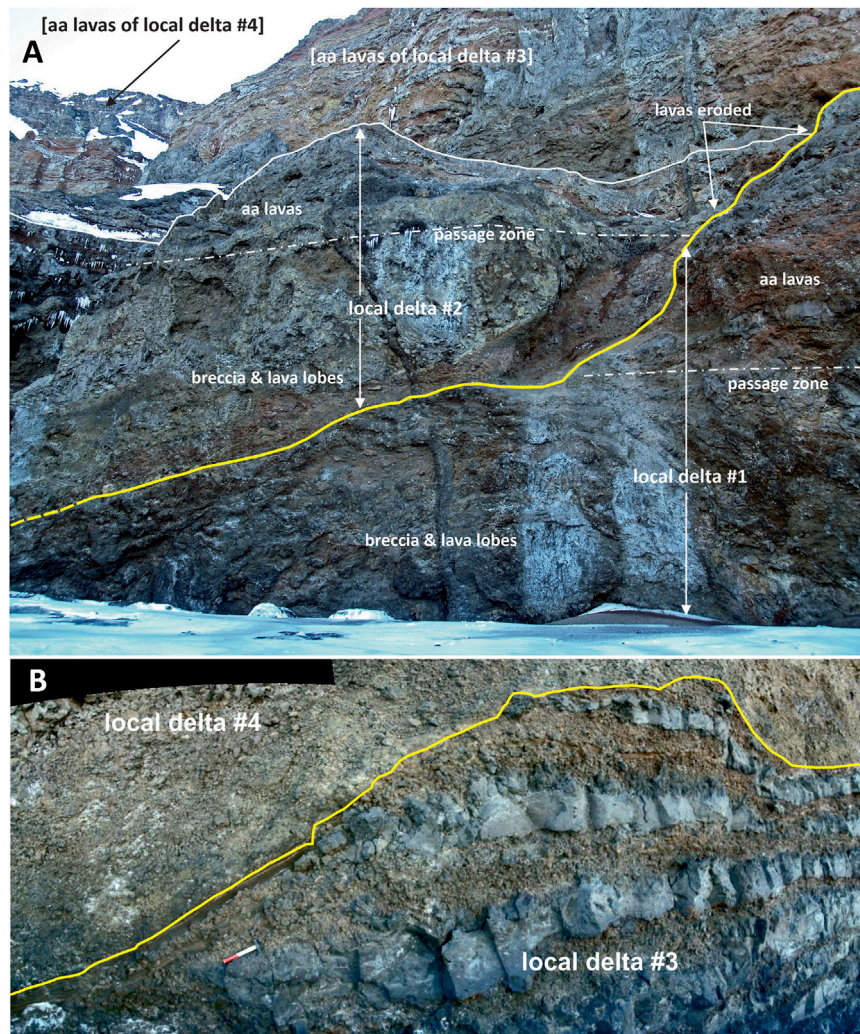
FIGURE 13
Views of upper eroded surfaces (bold yellow lines) of lava-fed deltas at Cape Washington. **(A)** Local lava-fed delta #1; the upper surface of delta #2 is inaccessible, and the uneven appearance is an effect of perspective. **(B)** Local lava-fed delta #3; the subaerial lava capping sequence of delta #3 is substantially thinner at this location (c. 20−25 m) than 0.5 km to the north, where it reaches at least 50 m in thickness (see Figure 5). The evidence for the erosion of the lava-fed delta surfaces suggests that they were modified by wet-based ice.

capping 'a'ā lavas, and their proportion often exceeds 90% in the uppermost several meters, corresponding to a passage zone, that is, a transition zone separating subaqueous from subaerial lithofacies (see Jones, 1969; Smellie and Edwards, 2016). Passage zones in 'a'ā lava-fed deltas are characteristically crudely defined.

5 Geochronology

We present 22 new $^{40}Ar/^{39}Ar$ ages for volcanic units at 19 localities, most dated for the first time (Figure 3; Table 2; Supplementary Figure S1). The new ages vary from 4.10 ± 0.12 to 0.063 ± 0.020 Ma. Lava-fed deltas at Cape Washington are stratigraphically consistent and range from 4.10 ± 0.12 Ma (delta #1) through 3.271 ± 0.039 Ma (delta #2) to 3.161 ± 0.011 Ma (delta #4). An additional $^{40}Ar/^{39}Ar$ step-heating analysis obtained on delta #4 at a different locality (Figure 11) proved to be slightly but significantly younger, at 2.903 ± 0.037 Ma, which is unexplained and might cast

doubt on the mapped correlation, although the units look identical and their elevations (including the passage zone) are comparable. The lava-fed delta that dominates the separate small shield volcano outcrop on the east side of the Cape Washington peninsula yielded an imprecise age of c. 1.8 Ma, whereas the lava-fed delta northwest of Edmonson Point is dated as 1.027 ± 0.006 Ma. The tuff cones show a wide age range, from $2.951 \pm .050$ Ma (northeast of Baker Rocks) to 0.063 ± 0.020 Ma (summit lava at Shield Nunatak), but most are of Pleistocene age ($\leq$ c 1.74 Ma). The megapillow complexes range in age from 0.907 ± 0.005 (southwest of Edmonson Point) to 0.128 ± 0.007 Ma and 0.127 ± 0.003 Ma (north of Edmonson Point). However, with an age for the megapillow complex outcrop at southern Edmonson Point published by Giordano et al. (2012) (0.298 ± 0.055 Ma), the ages collectively indicate that megapillow complexes in the MMVF were emplaced in multiple episodes at c. 0.91, c. 0.30, and c. 0.13 Ma. Scoria cones and associated intrusions (necks) and lava fields yielded ages of 2.913 ± 0.012 Ma and 1.657 ± 0.010 Ma (both near Cape Washington), 1.629 ± 0.013 Ma (lava underlying

Shield Nunatak), and 0.088 ± 0.004 Ma (young lava unconformably draping trachytic ignimbrite at Edmonson Point; Figure 8). The latter age is indistinguishable within uncertainties from those of 0.091 ± 0.019 Ma (Edmonson Point) and 0.112 ± 0.084 Ma (nunatak northwest of Edmonson Nunatak) obtained on likely correlative units by Giordano et al. (2012). There is no obvious association between the different eruptive types and any narrow time periods. All types erupted throughout the Late Pliocene and Pleistocene.

Finally, we dated an outcrop of trachytic ignimbrite at Edmonson Point. Its distinctive composition indicates that it was derived from the summit of Mount Melbourne. It has an age of 114.7 ± 2.8 ka. Our new age is close to but slightly younger than the mean age reported by Giordano et al. (2012) (124.3 ± 6.1 ka). Taking into account the slight increase in ages, if the most recent values for the reference minerals used by Giordano et al. (2012) are considered, our determination is not greatly dissimilar. We consider the c. 115 ka age a reliable estimate for the emplacement of the ignimbrite at Edmonson Point.

6 Discussion

6.1 Environmental conditions during eruptions in the Mount Melbourne Volcanic Field

The size, lithofacies, compositional uniformity, and internal architectures of the individual low-elevation outcrops in the MMVF examined in this study indicate that they are the products of small volcanoes (sensu White and Ross, 2011). They might also be called monogenetic, but for ancient eruptive centers, it is often impossible to distinguish the products of multiple eruptions in a single edifice. Studies of similar-sized centers often show that they had long histories of multiple eruptions separated by short breaks in activity. However, the lack of obvious internal erosional surfaces that could have been caused by an eruptive hiatus suggests that they are likely to be monogenetic. The construction and morphology of small volcanic centers are determined by internal and external factors. Internal factors include the composition and physical properties of the erupting magma (e.g., viscosity and volatile content). External factors include tectonic setting (differential stress) and magma input (production) rate, but these factors simply affect the size of an edifice [polygenetic (large) *versus* monogenetic (small)] (Takada, 1994). They do not determine the style of eruption or type of monogenetic edifice (e.g., scoria cone *versus* tuff cone). Other external factors are essentially environmental and include the presence and recharge rate of groundwater and surface water (lake, sea). The influence of environmental factors is reflected in the sequence architecture and features of the lithofacies (e.g., clast grading and morphology, clast types, joint patterns, and relative crystallinity).

6.1.1 Scoria cones

The lithofacies that form the small isolated scoria cones (i.e., oxidized scoria, agglutinate, and clastogenic lavas) and the association of some containing ʻaʻā lavas with oxidized autobreccias, or rarely pāhoehoe, are diagnostic of "dry" magmatic eruptions in the absence of surface water or groundwater. Given the polar setting (74°S–75°S), the region need not be entirely ice-free. However, it is possible, given the low elevation and coastal location of the MMVF (<1,500 m asl; mostly <500 m). Despite the widespread

extent of snow and ice affecting the MMVF today, the locations of the scoria cone outcrops consist of bedrock with a snow cover probably too thin to interact significantly with the erupting magmas. Likely, modern eruptions at many sites would also produce scoria cones with magmatic or "dry" lithofacies. Therefore, the eruption of the scoria cones indicates environmental conditions comparable with today or with less snow and ice. However, lavas that flow across the snow- or ice-covered ground should show signs of interaction, resulting in distinctive cooling joint patterns (Mee et al., 2006), although the evidence may be difficult to detect (Edwards et al., 2012). However, the apparent absence of such evidence at the localities visited implies that snow- and ice-free conditions probably prevailed at those localities.

6.1.2 Tuff cones

After scoria cones, tuff cones (Surtseyan) are the next most common edifice type. They are not diagnostic of the environment but are formed by the interaction of magma with surface water, either seawater or glacial meltwater, rather than groundwater. The topography surrounding the tuff cone outcrops is unable to pond freshwater, and pluvial lakes are, therefore, unlikely. From our argument earlier, the tuff cones were surrounded by water with a surface at a high elevation (elevations mainly varying between c. 200 m and c. 300 m above modern datum). If the source of the water was marine, it implies that the sea level was at a similar elevation. The Holocene marine limit in the Terra Nova region is c. 30 m asl (Baroni and Orombelli, 1991; Baroni and Hall, 2004; Rhee et al., 2020), similar to that in southern Victoria Land (Hall et al., 2004). Pre-Holocene (age uncertain) raised beaches are also known to be present in southern Victoria Land. However, the marine limit for the few currently described is still within the Holocene marine limit (Gardner et al., 2006). However, Rhee et al. (2020) described undated "very wide and flat benches [also described by the authors as terraces] with minor elevation variations" at elevations up to c. 200 m on Inexpressible Island (southwestern Terra Nova Bay, northern Victoria Land). From the lack of beach deposits and a surface composed of shattered bedrock and erratics, the surfaces were presumed by Rhee et al. (2020) to be glacial in origin. Although they may be a result of structurally controlled glacial erosion (personal communication from C Baroni, June 2022), there is no support from the underlying geology, which is composed of essentially isotropic plutonic rocks lacking horizontal planes of weakness that ice might have preferentially exhumed (Vincenzo and Rocchi, 1999; Rocchi et al., 2004). Alternatively, the flat terrace-like morphology might be relics of wave-cut platforms that were subsequently overridden, fractured, and otherwise modified by ice. Their interpretation as marine features has not been verified and is therefore speculative; if they have a marine origin and associated uplift, they will increase the likelihood that marine water may have been involved in the eruption of at least some of the tuff cones in the MMVF. An alternative source of water is meltwater created during glaciovolcanic eruptions, a scenario that was assumed by previous workers without supporting evidence (Wörner et al., 1989; Giordano et al., 2012), and we discuss this in the following paragraphs.

Distinguishing between seawater and glacial meltwater can be achieved in favorably exposed instances by examining the lithofacies and architecture of tuff cones. Because of the buttressing effects of coeval ice during glaciovolcanic eruptions, the tephra products rapidly infill the englacial (meltwater-filled) vault and bank up against the enclosing ice walls (Smellie, 2018, in press; Edwards et al., 2022). This leads to a distinctive edifice morphology with a high aspect ratio
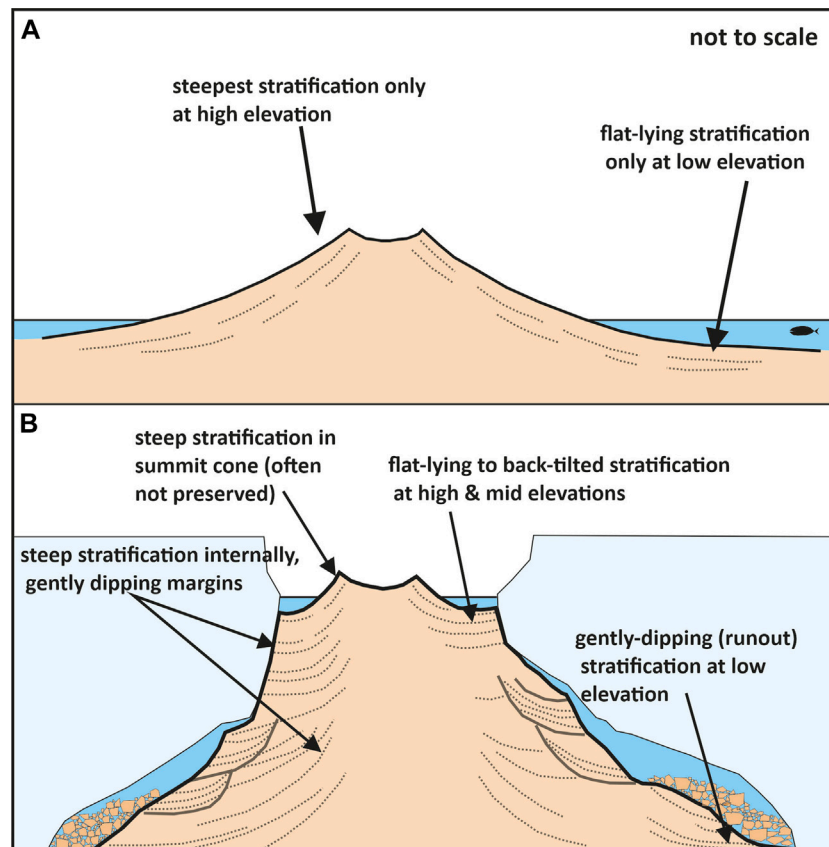
FIGURE 14
Schematic diagrams illustrating the contrasting morphologies and internal architectures of tuff cones erupted under **(A)** non-glacial, unconfined conditions (in the sea or a pluvial lake) and **(B)** glacial, confined conditions (i.e., under an ice sheet). **(A)** omits the effects of undercutting of tuff cones erupted in exposed locations, which can cause slumping and shear surfaces (illustrated in Figure 16), sometimes associated with beach deposits (White, 1996). Note how tuff cones constructed in ice also have higher aspect ratios (height:basal width; Smellie, 2013).

(i.e., limited lateral extent) and an internal architecture comprising gently dipping strata at all elevations around the margins of englacial tuff cones. As volcanic heat is transferred to the enclosing ice, the walls recede, thus removing their buttressing support and leading to repeated sector collapses of the tuff cone flanks. Glaciovolcanic tuff cones are characterized by prominent slump-scar surfaces (Smellie, 2001; Smellie, 2018). By contrast, eruptions in the sea (or in pluvial lakes) are unconfined, and the strata are laterally extensive and asymptotic, declining from c. 20° to 45° around the summit crater to almost horizontal in the subaqueous ring plain (Sohn, 1996; Smellie et al., 2018). These relationships are illustrated in Figure 14. Of course, marine-emplaced tuff cones constructed in exposed locations can also be undercut by wave activity and may collapse similarly to collapses that affect larger volcanic arc edifices (Moorhouse and White, 2016; Romero et al., 2021). The scarcity of descriptions of collapse features in small marine tuff cones suggests that they are seldom preserved (marine-emplaced tuff cones are typically short-lived features; Sohn, 1996; Kano, 1998; Cole et al., 2001; Solgevik et al., 2007; Cavallero and Cortelli, 2019; Garvin et al., 2018).

Tuff cone outcrops at Harrow Peaks, Baker Rocks (south), east of Willows Nunatak, and Shield Nunatak have features that appear to have been determined by eruptions through a glacial cover. The Harrow Peaks outcrop is inland and sits astride a sharp-crested, steep bedrock ridge with an elevation of c. 360–400 m asl. There is

abundant evidence for water saturation of the tephra pile, including the presence of coeval water-cooled hypabyssal intrusions with fluidal margins. The characteristics have been interpreted as diagnostic of eruption in a meltwater lake perched atop the ridge, which was covered by cold-based ice during the eruption to confine the meltwater in a vault on top of a steeply dipping (50–70°) bedrock (Smellie et al., 2018). The other three outcrops show lapilli tuff strata that are essentially flat-lying at high elevations in the outcrops, and strata at Shield Nunatak also frequently dip in toward the center of the nunatak (Figures 6, 7). These observations are inconsistent with unconfined eruption and suggest that the tephra piles occupied and infilled an englacial vault, with the tephra banked against the ice walls (Figure 14B). Moreover, water-cooled (entablature) jointing affects coeval hypabyssal intrusions up to high elevations, and one outcrop (Baker Rocks, south) has intrusive pillow lava between 400 and 600 m asl. Hence, the tephra piles were water saturated to similar heights. All three outcrops are also associated with coarse grey scoria lapillistones. The scoria deposits occur at the top (Baker Rocks south; Shield Nunatak), within (Shield Nunatak), and at the exposed base (east of Willows Nunatak; Figures 6, 7) of the outcrops. The summit of Baker Rocks (south) is a small scoria cone. It is draped by a thin cover of fine lapilli tuffs that were probably sourced from the crater responsible for the adjacent outcrop at Baker Rocks (north), consistent with the c. 1 Myr age difference between the two centers
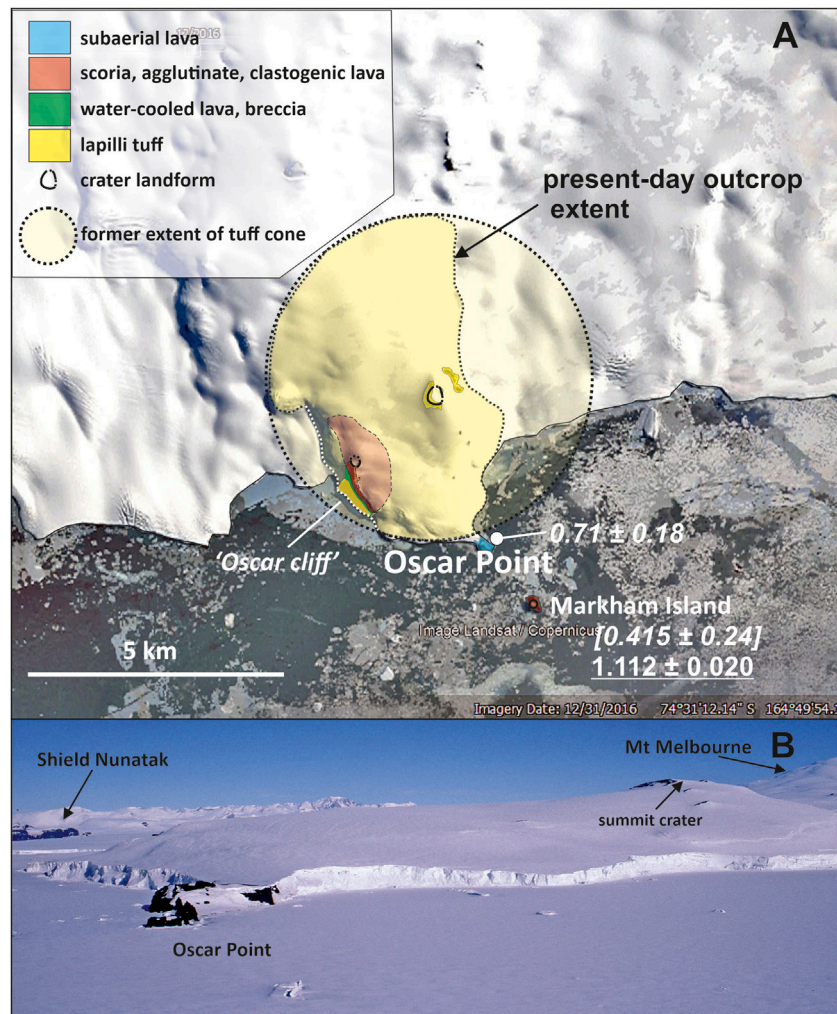
FIGURE 15
(A) Map of Oscar Point showing the inferred original extent of the tuff cone that forms most of the locality. **(B)** Photo of Oscar Point looking northwest, showing the very low gradient of the tuff cone flanks compared with steeper gradients rising to the cratered summit area. Evidence for pervasive water-cooling of coeval intrusions occurs up to c. 180 m asl in "Oscar cliff," suggesting that the contemporary sea level reached a similar elevation. See Figure 16 for a view of the tuff cone strata and syn-eruptive deformation at "Oscar cliff." Satellite image courtesy of Google Earth (data provider Landsat/Copernicus, 2016).

(Supplementary Figure S1). Summit scoria cones are a common feature of tuff cones and form as the vents dry out (Wohletz and Sheridan, 1983; Sohn, 1996; Cole et al., 2001; Solgevik et al., 2007; Smellie et al., 2018). However, the prominent necks intruding scoria lapillistones at northeast Shield Nunatak and the outcrop east of Willows Nunatak are entablature jointed, indicating that the scoria deposits were water-saturated by the time the necks intruded. We concur with Wörner et al. (1989) that the occurrence of "dry" scoria deposits within lapilli tuff successions in the MMVF was due to variable water levels within the englacial cavities during eruptions. They are incompatible with an origin by eruptions in an unconfined setting.

By contrast, the tuff cone at Oscar Point (Figure 15) has a broad shield morphology with low flank gradients steepening up to a small summit cone, suggesting eruption in an unconfined setting. The outcrop also shows spectacular syn-eruptive deformation, comprising disturbed bedding and numerous shear surfaces along which strata have slipped (Figure 16). The features are consistent with undercutting and slope collapses (slides, slumps) triggered by

contemporary marine erosion, or else collapses of bedding over-steepened in the summit region of the tuff cone followed by redeposition at lower elevations (Sohn, 1996). Water-cooled intrusive sheets also occur at c. 180 m asl (estimated; Figure 15A) and extend to lower levels as irregular masses, indicating a high coeval sea level. By contrast, it is difficult to assign an eruptive setting unambiguously to tuff cone outcrops northeast of Baker Rocks and north of Willows Nunatak. Both appear to fit well with a model of unconfined eruptions, presumably in seawater, as a lacustrine setting is excluded (lack of suitable palaeotopography to pond water). They contain strata with variable dips (<5–24) that appear to extend laterally 750 m to more than 1 km. Bed orientations in the outcrop northeast of Baker Rocks indicate that at least two eruptive centers were active, probably simultaneously, and a crater-rim unconformity is preserved in high elevation exposures (above c. 350 m asl) of the more southwesterly center. The age of the Oscar Point tuff cone is unknown, but the ages of the other two (2.951 ± 0.050 Ma, 0.756 ± 0.023 Ma; Table 2) correspond to relatively low $\delta^{18}O$ values consistent
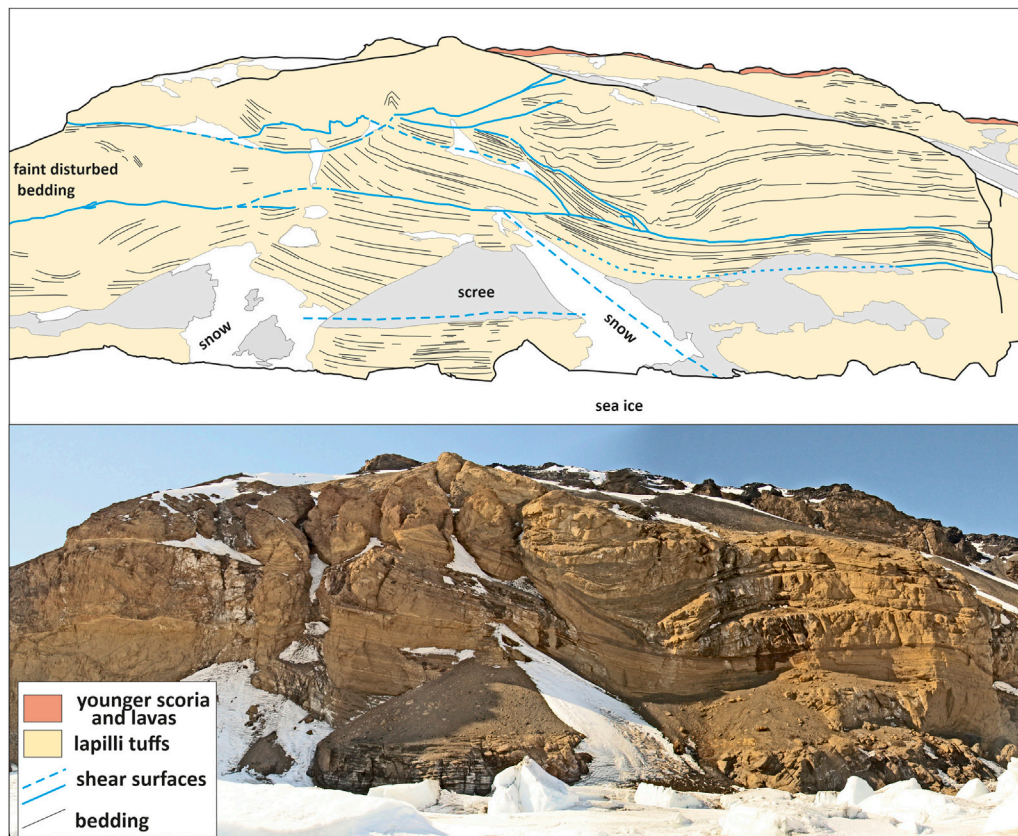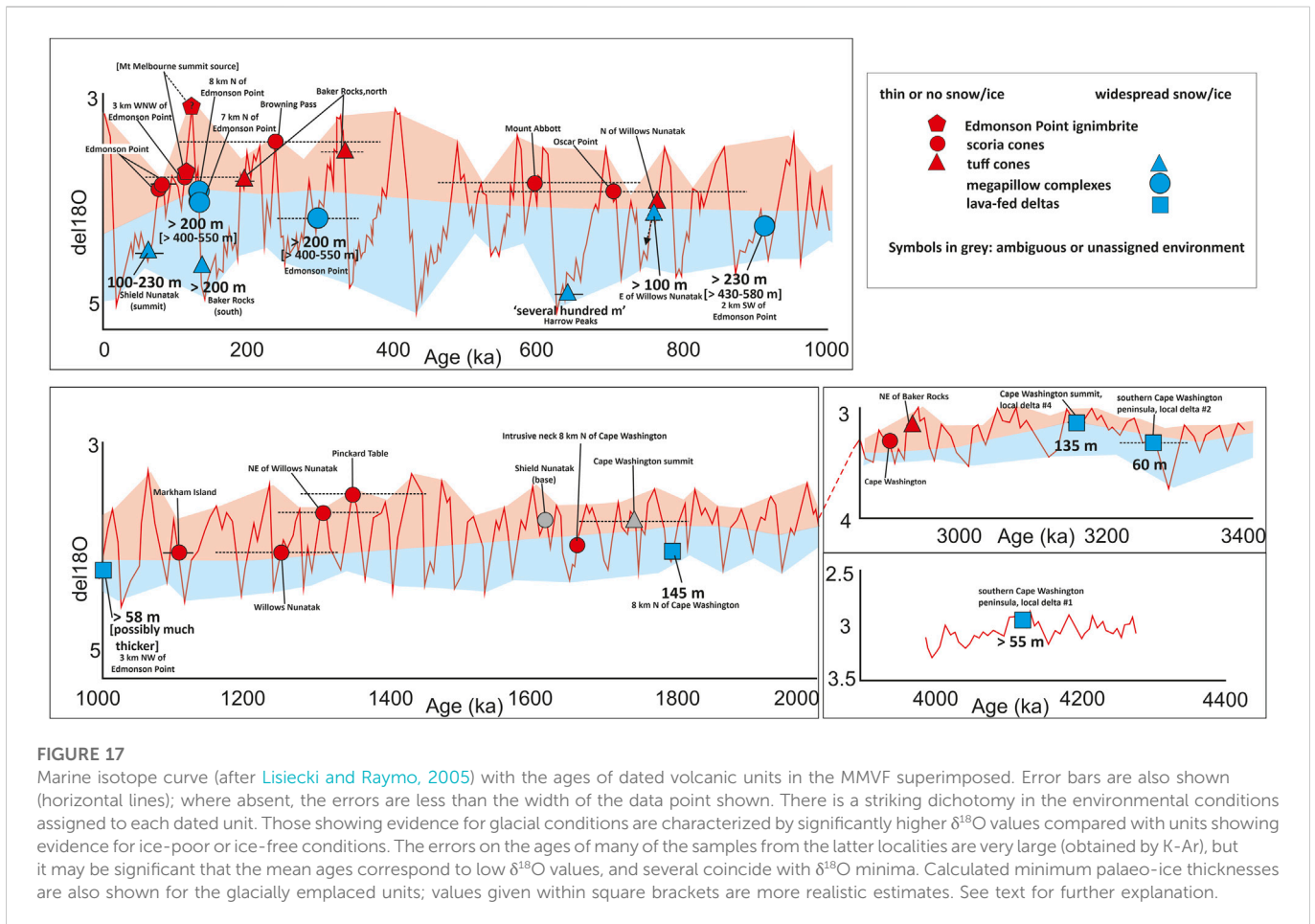
FIGURE 16
Sketch and photograph of "Oscar cliff" showing gently dipping bedding with multiple shear surfaces and associated localized folding caused by contemporary marine undercutting causing instability or over-steepened bedding in the summit region that collapsed and was redeposited near the toe of the tuff cone. The capping unit of scoria and lavas shown is unrelated to the tuff cone. The height to the skyline is c. 180 m.

with an interglacial period (Figure 17). All three localities are also situated on the coast. The evidence is most consistent with eruptions that were unconfined and affected by seawater that extended over each of the sites. However, as indicated earlier, there is currently no unambiguous corroborating evidence for substantially higher sea levels (up to c. 200 m asl) during the eruption of the tuff cones. The environment during the eruption of the outcrop at Baker Rocks (north) is also equivocal. It shows steeply dipping (28) strata where a crater-rim unconformity is exposed high in the outcrop. Ash-coated lapilli are also present in the lapilli tuffs above c. 500 m asl. The age of the outcrop is not well defined, with two options of 0.33 ± 0.03 or 0.20 ± 0.01 Ma (by K-Ar; Supplementary Figure S1). Both possible ages have high errors but correspond to periods of relatively low $\delta^{18}O$ values, likely interglacial (Figure 17; and see Section 6.3). The outcrop location is further inland than the other three tuff cones. In the absence of a palaeotopography suitable for ponding a pluvial lake, the source of contemporaneous water would have to be either the sea or a free-flowing aquifer readily recharged by seawater (Sohn, 1996). The bedrock underneath the outcrop is likely composed of Palaeozoic granitoids or siliceous Beacon Supergroup sedimentary strata, neither of which appear to be good candidates for a free-flowing aquifer (Nathan and Schulte, 1968). However, an unknown fault zone could act as a proxy aquifer. Thus, the environment is equivocal, and with so little lateral extent of the outcrop preserved, a glacial setting is not precluded.

6.1.3 Megapillow complexes

The topography surrounding the megapillow complexes in the MMVF is incapable of ponding water in a pluvial lake. From our discussion above, if the sea level was substantially higher in the past, eruptions might thus have been submarine. The suggestion is unverified at present, but a marine setting during the emplacement of the megapillow complexes is thought to be unlikely for the reasons presented below. Conversely, eruption beneath ice could also create a meltwater lake into which the megapillow complexes were emplaced, and the polar location of the MMVF (74°S) makes a glacial setting a plausible option. Pillow mounds and ridges are well-known as glaciovolcanic edifices (Höskuldsson et al., 2006; Edwards et al., 2009; Smellie, 2013; Pollock et al., 2014) and also in submarine settings (Schmincke and Bednarz, 1990; Goto and McPhie, 2004), but megapillow complexes like those in the MMVF have not yet been described. Megapillows were described in a subglacial lava field in British Columbia, but they are volumetrically minor. They were regarded as feeder tubes for associated pillow lavas (Hungerford et al., 2014). However, that outcrop also contains lithofacies called massive lavas, comprising low oblate lava lobes up to 3 m thick and 2–15 m long showing entablature prismatic jointing overlying suppressed colonnades and locally with hackly jointed upper surfaces. The features closely resembled our lava lobes and were similarly attributed to enhanced magma discharge rates. However, they occur in a geographically restricted part of a lava field rather than

FIGURE 17
Marine isotope curve (after Lisiecki and Raymo, 2005) with the ages of dated volcanic units in the MMVF superimposed. Error bars are also shown (horizontal lines); where absent, the errors are less than the width of the data point shown. There is a striking dichotomy in the environmental conditions assigned to each dated unit. Those showing evidence for glacial conditions are characterized by significantly higher δ^{18}O values compared with units showing evidence for ice-poor or ice-free conditions. The errors on the ages of many of the samples from the latter localities are very large (obtained by K-Ar), but it may be significant that the mean ages correspond to low δ^{18}O values, and several coincide with δ^{18}O minima. Calculated minimum palaeo-ice thicknesses are also shown for the glacially emplaced units; values given within square brackets are more realistic estimates. See text for further explanation.

as a major constituent of several prominent glaciovolcanic mounds composed of a plexus of megapillows, lava lobes, and lava sheets.

The unusual, irregular glass-lined cavities observed in the MMVF outcrops are interpreted here as ice-block melt-out cavities (Figure 9D), formed by the incorporation of ice blocks trapped by advancing lava (Skilling, 2009). Although a rare occurrence, their presence is highly significant as it argues against a submarine or pluvial lake in favor of a subglacial setting. Since ice floats, it implies that the meltwater did not form a deep lake but was at least partly drained to allow the ice block(s) to accumulate. This is also consistent with the presence of pumice lapillistones and stratified pumiceous lapilli tuffs. Pumice is likely to float and would be reworked by traction currents only if the vault meltwater was largely drained. However, the frequent occurrence of entablature jointing also indicates that the lava surfaces were rapidly chilled by water, here assumed to be meltwater. This conundrum may be explained if emplacement was within a subglacial vault that was largely drained but continually replenished by melting the ice roof and walls. The vault is envisaged actively draining basally; it was not entirely filled by meltwater. The higher magma discharge rates inferred for the complexes may have exerted positive pressures on the overlying ice, causing it to lift and facilitating basal meltwater drainage. The lavas were chilled by contact with ice and washed with water, but they were probably only partially immersed. Radiant heat from the cooling lava would cause the melting of the ice roof, and meltwater would flow freely over the lava surfaces. A similar scenario was proposed by Hodgetts et al. (2021) for subglacially emplaced,

water-cooled sheet lavas in an unusual tuya in Iceland. The tuya was constructed on a sloping bedrock surface, which promoted efficient subglacial drainage and a wet but not water-filled englacial vault. The colonnades in the megapillow complexes in the MMVF represent a slower, conductive cooling regime at the base of the thicker lava sheets, where they were in contact with earlier-emplaced lava, possibly still warm, and water was excluded (displaced). In places, lava overrode water-filled hollows in the underlying surface, causing breakouts and generating localized clusters of small lava pillows. Local minor instability of the pile was probably responsible for the generation of hyaloclastite, although the hyaloclastite was often reworked and redeposited by traction currents and occasional mass flows. The formation of minor interbedded pumice and lapilli tuffs in the megapillow complex at Edmonson Point, apparently deposited at different times during its growth, implied that explosivity was also sometimes achieved, with the explosively generated products reworked through the vault by currents and minor collapses of the tephra pile. Although explosivity can occur at high ambient pressures (by IFCI; Dürig et al., 2020), it is an unlikely explanation for the pumiceous lapilli tuffs at Edmonson Point, which contain abundant highly inflated pumices and lack the distinctive curviplanar ash-size shards that characterize IFCI deposits. The thickest tephra deposit (>20 m) caps the complex on top of the ridge on the west side of Edmonson Point, implying that explosivity may ultimately have succeeded effusion in the final stages of the eruption of that complex. Similar deposits are absent from the other megapillow

complexes in the MMVF, which presumably remained wholly effusive. However, the evidence for only partial immersion of the lava masses in water argues against a submarine (wholly drowned) origin. A glaciovolcanic origin is the most plausible explanation for the eruptive setting.

6.1.4 Lava-fed deltas

Although lava-fed deltas are not environment-specific, there are clear indications that they formed in association with ice in the MMVF. The passage zones in the lava-fed deltas on the Cape Washington peninsula have an overall gentle southerly or southwesterly dip. As water levels in the sea and pluvial lakes are horizontal, the presence of dipping passage zones in the Cape Washington peninsula deltas is diagnostic of emplacement on the flanks of volcanoes draped by ice (Smellie et al., 2011b; Smellie, 2018). The gentle dips also indicate that the original volcanoes were shield-like in morphology, and the craters that fed the deltas were situated to the east of the Cape Washington peninsula but have since been lost by a combination of glacial and marine erosion. Because the isolated delta outcrop north of Edmonson Point is small and its capping lavas were removed by erosion, the orientation of the delta and its passage zone is unclear. Although the delta prograded to the east, indicating a source vent somewhere to the west, it may have erupted in a glacial, pluvial lake or marine setting. However, the two prominent subhorizontal bands of pervasive alteration observed in the associated lithic breccias close to the passage zone (Figure 9H) are likely to have formed due to prolonged immersion in water that underwent a change in surface elevation at least once. Delta advancement in a pluvial lake or into the sea would show only a single horizontal alteration front reflecting a sea or lake surface that would have been invariable during the eruption. The presence of two alteration zones, interpreted as two different former water levels, suggests that the water responsible for the alteration was dynamic, and its surface fluctuated with time due to subglacial meltwater discharge (Smellie, 2006). The likeliest eruptive scenario, therefore, is glaciovolcanic, with emplacement in wet-based ice. The former presence of wet-based ice during the eruption of the Cape Washington peninsula deltas is also supported by eroded surfaces between at least two of those deltas (deltas #1 and #3; Figures 13A, B).

6.1.5 Edmonson Point ignimbrite

Although not part of our study of the satellite and flank vents, the Edmonson Point ignimbrite, which erupted from Mount Melbourne summit, is an *in situ* pumiceous magmatic deposit that shows no evidence of water or ice interaction. Its presence, low elevation (essentially at sea level), and lack of evidence for subsidence had it been deposited on snow or ice indicate that it was deposited at an ice-free location, and the period was thus ice-poor or possibly ice-free (Figure 17; see section 7.3).

6.2 Effect of eruptive environment on eruptive style and edifice construction

The range of compositions overlaps for each of the edifice types in the MMVF and, apart from a bias to tephrite/basanites for the lava-fed deltas (Figure 2), there are no obvious compositional differences that explain the markedly different styles of eruption represented. Although many of the scoria cones are at relatively high elevations

(e.g., above 1,200 m in Random Hills; Figure 3), they also occur close to sea level. The other types of flank and satellite vents occur at similar elevations to the scoria cones (i.e., mostly <600 m asl), and relative elevation (with respect to potential interaction with marine water) is not the dominant determining factor for eruptive style. A major conclusion of our study is that the principal determinant for volcanic eruptions and edifice construction in the MMVF is environmental, specifically the presence at the eruptive sites of water in all its forms (snow, ice, meltwater, and surface water). Figure 18 schematically shows the relationships between the principal lithofacies, internal architectures, and edifice construction for centers that erupted in various environmental settings. For example, an absence of water or insufficient snow/ice at eruptive sites in the MMVF resulted in scoria cones and their associated lava fields. Most of the tuff cone outcrops visited show strong evidence for eruption within the ice, including gently and sometimes inward-dipping summit strata at high elevations and evidence for water saturation of the tephra piles at high elevations. However, the characteristics of a few tuff cone outcrops are more ambiguous and possibly fit better with eruptions in an unconfined setting (i.e., laterally continuous strata, steep-dipping in summit areas), with a water source potentially provided by the sea. This is particularly true for the Oscar Point tuff cone (Figure 15). Moreover, their ages appear to correspond to warmer periods compared with the marine $\delta^{18}O$ curve (Figure 17; and see Section 6.3) when ice extent would have been reduced and sea levels higher than today. However, independent corroborating evidence for the substantially higher sea levels required is currently lacking. Distinguishing between glacial and non-glacial settings reliably for tuff cones depends on reconstructing the internal architecture and, ideally, the original morphology of the tephra piles, which are not always possible for outcrops that are highly eroded or largely obscured by snow and ice. Effusive eruptions associated with a thin slope-draping glacial cover (<c. 150 m thick for the MMVF) created several small shield volcanoes constructed from multiple 'a'ā lava-fed deltas, mainly in the Cape Washington peninsula area. Similar examples also crop out extensively elsewhere in Victoria Land (Smellie et al., 2011a; Smellie et al., 2011b; Smellie et al., 2013; Smellie, 2021). By contrast, effusive eruptions associated with high magma discharge rates and a much thicker glacial cover (several to many hundreds of meters; see Section 6.4) created the distinctive megapillow complexes. Under similarly thick ice but lower magma discharge rates, pillow lava mounds would be formed.

6.3 Comparison with the marine oxygen isotope record

The arguments given above for eruptive settings are based solely on interpretations of the lithofacies present and their architecture. However, considerable ancillary support is also provided by the ages of the outcrops when they are plotted on the marine $\delta^{18}O$ isotope curve (Figure 17). Only two outcrops we visited have no eruptive environment currently assigned due to inconclusive lithofacies and architectures. The remaining outcrops are designated as "glacial" (lava-fed deltas; megapillow complexes; several tuff cones) and "non-glacial" (scoria cones and associated lava fields; possibly some other tuff cones). It is probably significant that despite the high errors on some of the published ages (most determined by imprecise K-Ar), all of the unambiguously "glacial" outcrops have ages corresponding to
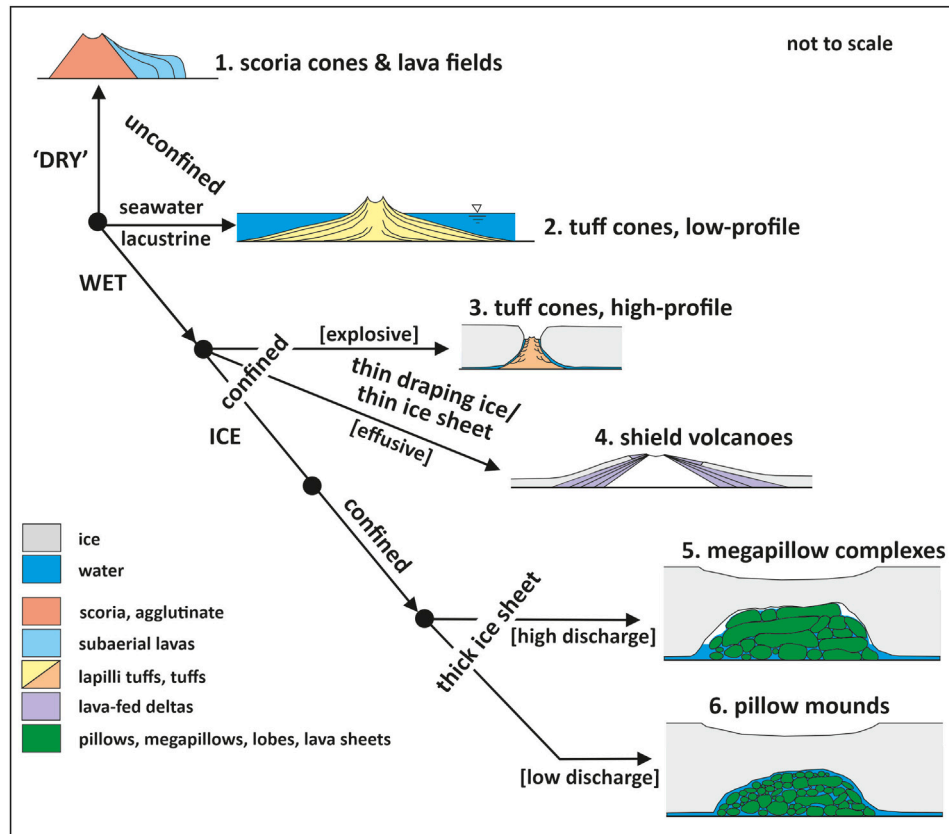
FIGURE 18
Schematic diagrams illustrating the impact of water on resulting edifice type under a range of environmental conditions. The presence or absence of water, including ice and its thickness, is the principal determinant of edifice construction. Note that glaciovolcanic (i.e., high-profile) tuff cones (category 3) can probably evolve into shield volcanoes draped by lava-fed deltas (category 4). The diagram also includes pillow mounds (category 6). Although not present in the MMVF, they are more common in glaciovolcanic settings generally and are likely to form under lower magma discharge rates than those that yield megapillow complexes.

relatively high $\delta^{18}O$ values on the marine isotope curve, whereas the "non-glacial" outcrops correspond in age to significantly lower $\delta^{18}O$ values. Only one outcrop conflicts with this conclusion: an intrusive neck c. 8 km north of Cape Washington (Figure 17). The constituent "lithofacies unequivocally indicate "dry' magmatic eruptions and a non-glacial or at least ice-poor setting, but the equivalent value on the $\delta^{18}O$ curve is relatively high (Figure 17). However, the outcrop age corresponds to a steep section of the $\delta^{18}O$ curve. Thus, the simplest explanation is that even a slight change in the age (by only a few ka) could displace it to substantially lower $\delta^{18}O$ values on the curve and remove the conflict. For the few tuff cones in the MMVF that might have erupted within the sea, a similar argument applies, thus emphasizing the ambiguity of the interpretation currently assigned to those outcrops. Finally, it is noticeable that within the constraints of the errors attached to the ages [which are very small (mainly 20–30 Kyr) in our new age dataset], the eruptions of units that experienced "glacial" conditions fall on the steep rising limbs of the $\delta^{18}O$ curve corresponding to periods of rapid ice melt, either glacial to interglacial transitions or a change to interstadials (Figure 17). Such a trend is a predicted consequence of the warmer climatic conditions lowering the superimposed glaciostatic load and triggering eruptions (Jull and McKenzie, 1996; Maclennan et al., 2002; Jellinek et al., 2004; Watt et al., 2013; Wilson and Russell, 2020).

6.4 Contemporaneous ice thicknesses

Empirical estimates for contemporaneous ice thicknesses are also shown in Figure 17. For each of the Cape Washington peninsula lava-fed deltas near Cape Washington, calculated ice thicknesses are >55, 55, 60, and 135 m (oldest delta to youngest, respectively). The additional younger delta 9 km north of Cape Washington was associated with ice c. 145 m thick, whereas the isolated delta relict north of Edmonson Point is too poorly exposed for an estimate. Calculations for the deltas are based on the observed thickness of subaqueous lithofacies to which is added c. 30 m to allow for any superimposed snow, firn, or crevassed ice (see Smellie et al. 2011b). The calculated thicknesses are minima as no allowance is made for ice surface sagging, but any sagging would be confined principally to the vicinity of the edifice; see Smellie et al. (2011b) for details of assumptions used in calculations. Other putative ice thicknesses at the eruptive sites are as follows:

1) Megapillow complexes: >200 m (i.e., the individual thickness of most of the megapillow complexes) but probably much thicker; for example, the coeval ice surface for the highest outcrop (west-northwest of Edmonson Point) must have substantially exceeded 400 m asl, which is the elevation of its preserved surface. The

thicknesses shown in Figure 17 are minima and based on the maximum elevation reached by the individual outcrops (but see further comments below).

2) Tuff cones: thicknesses calculated for glacially emplaced tuff cones vary between >100 m (east of Willows Nunatak) and several hundred meters (Harrow Peaks; see Smellie et al., 2018).

The estimates calculated for the lava-fed deltas and Shield Nunatak are the most accurate and are unlikely to be incorrect by more than a few tens of meters because the bases and original tops of most of the outcrops are exposed and the outcrops are capped by lavas that were emplaced subaerially. Hence, the coeval ice was melted through completely.

Estimates for the other landforms are probably less accurate, particularly for the megapillow complexes emplaced entirely subglacially. Two scenarios are possible for the complexes. (1) In undegassed magmas, the coeval ice thicknesses would have been substantial [i.e., much greater than the preserved thicknesses (mainly c. 200 m) of the individual complexes] to suppress runaway vesiculation triggering explosivity, whether magmatic or hydrovolcanic. Thus, for a complex 200 m thick, the minimum thickness of contemporary ice would have been c. 550 m (comprising 200 m of magma and 200 m of superimposed ice plus c. 150 m to account for ice surface sag toward the complex; see Gudmundsson, 2003; Smellie et al., 2011b). The elevation of the highest megapillow complex surface is c. 400 m asl (nunatak west-northwest of Edmonson Point). It is an eroded surface; hence, it must have been higher originally. Similar reasoning suggests that the coeval ice surface would have had a minimum elevation of c. 750 m asl (i.e., 400 + 200 + 150 m). This is the thickest ice sheet for which volcanic rocks in the MMVF provide evidence. However, for that example, if uplift has subsequently occurred (although undocumented at present), the deduced surface elevation and associated ice sheet thickness would need to be reduced. Since the megapillow complex at Edmonson Point shows an upward transition to explosive activity, the coeval ice thickness is better defined and any overlying ice would not be greater than c. 200 m thick. The exposed thickness of the complex at the locality is c. 200 m; hence, the maximum ice thickness there during effusion was ≤ 550 m.

Alternatively, (2) if the magmas were degassed and emplaced in a partially drained vault, the ambient pressures would have been much less than those imposed by the superimposed ice and might even have been atmospheric if the vault drained to the ice sheet margins (*cf.* Schopka et al., 2006; Wilson et al., 2013). Low vault pressures (equivalent to less than c. 200 m of superimposed ice) would have promoted pervasive vesiculation and a rapid transition to explosive (hydrovolcanic) activity at an early stage, which is not observed. Hence, some of the magmas (not Edmonson Point) might have been degassed when emplaced. However, the presence of vesicle zones signifying inflation, together with megavesicles, suggest that the magmas were not degassed.

Even if it was assumed (1) that the magmas were degassed and that c. 50 m of ice remained above the cooling complex (to avoid subaerial exposure) and (2) that the ice also sagged toward the cooling magma mass, the megapillow complexes that were c. 200 m thick would have been emplaced below the ice that was at least 400 m thick (i.e., 200 + 50 + 150 m). Whichever assumptions are used, the estimates indicate that substantially thicker ice conditions existed during the emplacement of the megapillow complexes than occurs at those locations today (see also Smellie et al., 2018). However, even the maximum calculated ice thicknesses would be unable to completely drown the topography of the region (Random Hills rise to >1,500 m asl, and the summit of Mount Melbourne is at 2,732 m). The ice cover indicated is, therefore, relatively thin overall, suggesting that it was mainly an icefield during the past 4 Myr. This does not preclude transient episodes of greater ice thicknesses at times when the ice overrode much of the topography (see Smellie et al., 2018), but those episodes are not represented by the volcanic record, and they were atypical for the bulk of the period represented.

7 Conclusions

The Late Pliocene to present Mount Melbourne Volcanic Field has a diversity of flank and satellite volcanic centers unrivaled anywhere else in the West Antarctic Rift System. Based on the lithofacies and internal architectures, several discrete groups of volcanic edifices are present, comprising scoria cones (together with their associated lava fields), possibly two types of tuff cones, megapillow complexes, and shield volcanoes constructed from lava-fed deltas. The diversity of edifice types is not related to compositional differences, which overlap completely (tephrite/basanite/alkali basalt–benmoreite) or due to elevation differences relative to any putative source of surface water (e.g., the sea) as the edifices crop out over a similar range of elevations. However, contemporary environmental conditions appear to have exerted the strongest control on eruptive style and, thus, edifice construction, specifically the presence or absence of water, including ice and its thickness. Eruptions under "dry" conditions created scoria cones and associated small lava fields (mainly 'a'ā lavas). Conversely, if some eruptions occurred under wet unconfined (e.g., submarine) conditions, tuff cones would be constructed composed of laterally extensive lapilli tuff strata with low-gradient flanks. However, the unconfined tuff cone eruptions, which appear to be unequivocal for the low-profile, shield-like Oscar Point tuff cone, require a high marine limit (at least 200 m above present datum), probably linked to local uplift, which is currently unverified. The suggestion thus requires independent validation. Three categories of glaciovolcanic edifices were also created depending on whether the eruptions occurred under thin (≤ c. 200 m) or much thicker ice. Under conditions of thin draping ice, effusive eruptions formed glaciovolcanic shield volcanoes composed of multiple 'a'ā lava-fed deltas, whereas explosive eruptions formed tuff cones with distinctive gently or inward-dipping strata at high elevations in flooded tephra piles due to banking of the strata against surrounding buttressing ice walls. One of the glaciovolcanic tuff cones (Shield Nunatak) has a weakly developed cap of sheet-like 'a'ā lavas, and it is transitional to a tuya. Eruptions under ice that was thick enough to suppress explosivity in undegassed magmas created sizeable megapillow complexes, a distinctive category of glaciovolcanic edifice that has not been described previously. They probably erupted into partially drained englacial vaults at moderately high discharge and relatively slow cooling rates. Thus, our study demonstrates that other than the abundant scoria cones and associated small lava fields, the Plio-Pleistocene centers in the MMVF are mainly glaciovolcanic, but they were constructed under a range of environmental conditions.

The volcanic units indicate that contemporary ice thicknesses at times were <55 m, but ice surfaces reached 750 m asl at one site, at least, at other times, much higher (therefore thicker ice) than at that site today. Eruptions of the glacially emplaced units are mostly biased

to periods of rapid ice thinning during deglaciation. The glacial thermal regime varied between wet-based (megapillow complexes and at least some lava-fed deltas; with evidence for basal meltwater discharge or erosion) and cold-based (tuff cone at Harrow Peaks, with an absence of basal meltwater discharge). With the much-improved dating precision, it appears that several glaciovolcanic edifices erupted at or close to glacial maxima. In the absence of other data, they are our best guide to past terrestrial palaeo-ice thicknesses and glacial thermal regime in the Terra Nova Bay region of northern Victoria Land. They indicate that the Late Pliocene and Pleistocene ice was generally quite thin and would have draped the landscape as an icefield rather than completely or largely drowning the topography as an expansive ice sheet. Although transient thicker ice probably occurred at times, it is not well represented. It is also noticeable that the ice became significantly thicker as δ^{18}O values increased toward the present. Finally, even during the earliest volcanic eruptions, at c. 4.1 Ma, when δ^{18}O variations were very limited and δ^{18}O values were slightly lower than today, the evidence indicates that an ice cover was present in the MMVF, although probably very thin at that time (just a few tens of meters at the coast). Thus, the volcanic record suggests that ice was probably never completely absent throughout the period investigated.

Data availability statement

The datasets presented in this study can be found in online repositories (see Supplementary Material).

Author contributions

JS: conceptualization (lead), data acquisition (lead), data curation (equal), formal analysis (lead), investigation (lead), writing—original draft (lead), writing—review and editing (lead). SR: funding acquisition (lead), conceptualization (supporting), data acquisition (equal), data curation (equal), formal analysis (supporting), investigation (supporting), writing—original draft (supporting), writing—review and editing (supporting). GD: conceptualization (supporting), data acquisition (equal), data curation (equal), formal analysis (supporting), investigation (supporting), writing—original draft (supporting), writing—review and editing (equal).

Funding

Acknowledgments

Conflict of interest

The authors declare that the research was conducted in the absence of any commercial or financial relationships that could be construed as a potential conflict of interest.

Publisher's note

All claims expressed in this article are solely those of the authors and do not necessarily represent those of their affiliated organizations or those of the publisher, the editors, and the reviewers. Any product that may be evaluated in this article, or claim that may be made by its manufacturer, is not guaranteed or endorsed by the publisher.

Supplementary material

The Supplementary Material for this article can be found online at: https://www.frontiersin.org/articles/10.3389/feart.2022.1061515/full#supplementary-material

SUPPLEMENTARY FIGURE S1
Satellite image of the Mount Melbourne Volcanic Field with all isotopic ages.

SUPPLEMENTARY FIGURE S2
Map showing the localities visited.

SUPPLEMENTARY FIGURE S3
Dating methods and results.

References

Allen, C. C. (1980). Icelandic subglacial volcanism: Thermal and physical studies. *J. Geol.* 88, 108–117. doi:10.1086/628478

Armienti, P., Civetta, L., Innocenti, F., Manetti, P., Tripodo, A., Villari, L., et al. (1991). New petrological and geochemical data on Mt. Melbourne volcanic field, northern Victoria Land, Antarctica. (II Italian antarctic expedition). *Mem. della Soc. Geol. Ital.* 46, 397–424.

Armstrong, R. L. (1978). K–Ar dating: Late cenozoic McMurdo volcanic group and dry valley glacial history, Victoria Land, Antarctica. *N. Z. J. Geol. Geophys.* 21, 685–698. doi:10.1080/00288306.1978.10425199

Baroni, C., and Hall, B. L. (2004). A new Holocene relative sea-level curve for Terra Nova Bay, Victoria Land, Antarctica. *J. Quat. Sci.* 19, 377–396. doi:10.1002/jqs.825

Baroni, C., and Orombelli, G. (1991). Holocene raised beaches at Terra Nova Bay, Victoria Land, Antarctica. *Quat. Res.* 36, 157–177. doi:10.1016/0033-5894(91)90023-x

Batiza, R., Smith, T. L., and Niu, Y. (1989). Geological and petrologic evolution of seamounts near the EPR based on submersible and camera study. *Mar. Geophys. Res.* 11, 169–236.

Batiza, R., and White, J. D. L. (2000). "Submarine lavas and hyaloclastite," in *Encyclopedia of volcanoes*. Editor H. Sigurdsson 1st edition (Sand Diego: Academic Press), 361–381.

Beccaluva, L., Coltorti, M., Orsi, G., Saccani, E., and Siena, F. (1991). Basanite to tephrite lavas from Melbourne volcanic province, Victoria Land, Antarctica. *Mem. della Soc. Geol. Ital.* 46, 383–395.

Bondre, N. R., Duraiswami, R. A., and Dole, G. (2004). Morphology and emplacement of flows from the deccan volcanic province, India. *Bull. Volcanol.* 66, 29–45. doi:10.1007/s00445-003-0294-x

Bonnichsen, B., and Kauffmann, D. F. (1987). "Physical features of rhyolite lava flows in the Snake River Plain volcanic province, southwestern Idaho," in *The emplacement of silicic domes and lava flows*. Editor J. H. Fink (Washington, DC: Geological Society of America Special Paper), 212, 119–145.

Brand, B. D., and Clarke, A. B. (2009). The architecture, eruptive history, and evolution of the Table Rock Complex, Oregon: From a Surtseyan to an energetic maar eruption. *J. Volcanol. Geotherm. Res.* 180, 203–224. doi:10.1016/j.jvolgeores.2008.10.011

Branney, M. J., and Kokelaar, P. (2002). *Pyroclastic density currents and the sedimentation of ignimbrites*, 27. London, Memoirs: Geological Society, 143.

Brown, R. J., Bonadonna, C., and Durant, A. J. (2012). A review of volcanic ash aggregation. *Phys. Chem. Earth* 45-46, 65–78. doi:10.1016/j.pce.2011.11.001

Cas, R. A. F., and Simmons, J. M. (2018). Why deep-water eruptions are so different from subaerial eruptions. *Frontiers in Earth Science*, 6, 198. doi:10.3389/feart.2018.00198

Cavallaro, D., and Coltelli, M. (2019). The Graham volcanic field offshore southwestern Sicily (Italy) revealed by high-resolution seafloor mapping and ROV images. *Front. Earth Sci.* 7, 311. doi:10.3389/feart.2019.00311

Chadwick, W. W., Cashman, K. V., Embley, R. W., Matsumoto, H., Dziak, R. P., de Ronde, C. E. J., et al. (2008). Direct video and hydrophone observations of submarine explosive eruptions at NW Rota-1 volcano, Mariana arc. *J. Geophys. Res.* 113, B08S10. doi:10.1029/2007JB005215

Clague, D. A., and Paduan, J. B. (2009). "Submarine basaltic volcanism," in *Submarine volcanism and mineralization: Modern through ancient* (Quebec City, Canada: Geological Association of Canada), 41–60. Short Course 29-30 May 2008.

Cole, P. D., Guest, J. E., Duncan, A. M., and Pacheco, J.-M. (2001). Capelinhos 1957-1958, faial, azores: Deposits formed by an emergent surtseyan eruption. *Bull. Volcanol.* 63, 204–220. doi:10.1007/s004450100136

Del Carlo, P., Di Roberto, A., Di Vincenzo, G., authors, 5, Landi, P., Pompilio, M., et al. (2015). Late pleistocene–holocene volcanic activity in northern Victoria Land recorded in Ross Sea (Antarctica) marine sediments. *Bull. Volcanol.* 77, 36. doi:10.1007/s00445-015-0924-0

Dürig, T., White, J. D. L., Murch, A. P., authors, 7, Buttner, R., Mele, D., et al. (2020). Deep-sea eruptions boosted by induced fuel-coolant explosions. *Nat. Geosci.* 13, 498–503. doi:10.1038/s41561-020-0603-4

Edwards, B., Magnússon, E., Thordarson, T., Guðmundsson, M. T., Höskuldsson, A., Oddson, B., et al. (2012). Interactions between lava and snow/ice during the 2010 Fimmvörðuháls eruption, south-central Iceland. *J. Geophys. Res.* 117, B04302. doi:10.1029/2011JB008985

Edwards, B. R., Russell, J. K., and Pollock, M. (2022). Cryospheric impacts on volcano-magmatic systems. *Front. Earth Sci.* 10. doi:10.3389/feart.2022.871951

Edwards, B. R., Skilling, I. P., Cameron, B., Haynes, C., Lloyd, A., and Hungerford, J. H. D. (2009). Evolution of an englacial volcanic ridge: Pillow Ridge tindar, Mount Edziza volcanic complex, NCVP, British Columbia, Canada. *J. Volcanol. Geotherm. Res.* 185, 251–275. doi:10.1016/j.jvolgeores.2008.11.015

Fisher, R. V., and Schmincke, H.-U. (1984). *Pyroclastic rocks*. Berlin: Springer-Verlag, 465.

Forbes, A. E. S., Blake, S., McGarvie, D. W., and Tuffen, H. (2012). Pseudopillow fracture systems in lavas: Insights into cooling mechanisms and environments from lava flow fractures. *J. Volcanol. Geotherm. Res.* 245-246, 68–80. doi:10.1016/j.jvolgeores.2012.07.007

Forbes, A. E. S., Blake, S., and Tuffen, H. (2014). Entablature: Fracture types and mechanisms. *Bull. Volcanol.* 76, 1–13. doi:10.1007/s00445-014-0820-z

Fox, C. G., Murphy, K. M., and Embley, R. W. (1987). Automated display and statistical analysis of interpreted deep-sea bottom photographs. *Mar. Geol.* 78, 199–216. doi:10.1016/0025-3227(88)90109-0

Gambino, S., Armienti, P., Cannata, A., and authors, 5 (2021). *Mount Melbourne and mount rittmann*, 55. London, Memoirs: Geological Society, 741–758.

Gardner, N., Hall, B., and Wehmiller, J. (2006). Pre-holocene raised beaches at Cape Ross, southern Victoria Land, Antarctica. *Mar. Geol.* 229, 273–284. doi:10.1016/j.margeo.2006.01.006

Garvin, J. B., Slayback, D. A., Ferrini, V., 4 authorsGiguere, C., Asrar, G. R., et al. (2018). Monitoring and modelling the rapid evolution of Earth's newest volcanic island: *Hunga Tonga Hunga Ha'apai* (Tonga) using high spatial resolution satellite observations. *Geophys. Res. Lett.* 45, 3445–3452. doi:10.1002/2017gl076621

Giordano, G., Lucci, F., Phillips, D., Cozzupoli, D., and Runci, V. (2012). Stratigraphy, geochronology and evolution of the Mt. Melbourne volcanic field (north Victoria Land, Antarctica). *Bull. Volcanol.* 74, 1985–2005. doi:10.1007/s00445-012-0643-8

Go, S. Y., Kim, G. B., Jeong, J. O., and Sohn, Y. K. (2017). Diatreme evolution during the phreatomagmatic eruption of the Songaksan tuff ring, Jeju Island, Korea. *Bull. Volcanol.* 79, 23. doi:10.1007/s00445-017-1103-2

Goehring, L., and Morris, S. W. (2008). Scaling of columnar joints in basalt. *J. Geophys. Res.* 113, B10203. doi:10.1029/2007JB005018

Goto, Y., and McPhie, J. (2004). Morphology and propagation styles of Miocene submarine basanite lavas at Stanley, northwestern Tasmania, Australia. *J. Volcanol. Geotherm. Res.* 130, 307–328. doi:10.1016/s0377-0273(03)00311-1

Granot, R., and Dyment, J. (2018). Late cenozoic unification of east and west Antarctica. *Nat. Commun.* 9, 3189. doi:10.1038/s41467-018-05270-w

Gregg, T. K. P., and Fink, J. H. (1995). Quantification of submarine lava-flow morphology through analog experiments. *Geology* 23, 73–76. doi:10.1130/0091-7613(1995)023<0073:qoslfm>2.3.co;2

Griffiths, R. W., and Fink, J. H. (1992). Solidification and morphology of submarine lavas: A dependence on extrusion rate. *J. Geophys. Res.* 97, 19729–19737. doi:10.1029/92jb01594

Grossenbacher, K. A., and McDuffie, S. M. (1995). Conductive cooling of lava: Columnar joint diameter and stria width as functions of cooling rate and thermal gradient. *J. Volcanol. Geotherm. Res.* 69, 95–103. doi:10.1016/0377-0273(95)00032-1

Gudmundsson, M. T. (2003). Melting of ice by magma-ice-water interactions during subglacial eruptions as an indicator of heat transfer in subaqueous eruptions. *Am. Geophys. Union Geophys. Monogr.* 140, 61–72.

Hall, B. L., Baroni, C., and Denton, G. H. (2004). Holocene relative sea-level history of the southern Victoria Land coast, Antarctica. *Glob. Planet. Change* 42, 241–263. doi:10.1016/j.gloplacha.2003.09.004

Hamilton, W. (1972). The hallett volcanic province, Antarctica. Geological Survey Professional Paper 456-C, 59.

Hodgetts, A. G. E., McGarvie, D., Tuffen, H., and Simmons, I. C. (2021). The Thórólfsfell tuya, South Iceland – a new type of basaltic glaciovolcano. *J. Volcanol. Geotherm. Res.* 411, 107175. doi:10.1016/j.jvolgeores.2021.107175

Höskuldsson, A., Sparks, R. S. J., and Carroll, M. R. (2006). Constraints on the dynamics of subglacial basalt eruptions from geological and geochemical observations at Kverkfjöll, NE Iceland. *Bull. Volcanol.* 68, 689–701. doi:10.1007/s00445-005-0043-4

Houghton, B. F., and Hackett, W. R. (1984). Strombolian and phreatomagmatic deposits of ohakune craters, ruapehu, New Zealand: A complex interaction between external water and rising basaltic magma. *J. Volcanol. Geotherm. Res.* 21, 207–231. doi:10.1016/0377-0273(84)90023-4

Hungerford, J. D. G., Edwards, B. R., Skilling, I. P., and Cameron, B. I. (2014). Evolution of a subglacial basaltic lava flow field: Tennena volcanic center, Mount Edziza Volcanic Complex, British Columbia, Canada. *J. Volcanol. Geotherm. Res.* 272, 39–58. doi:10.1016/j.jvolgeores.2013.09.012

Jellinek, A. M., Manga, M., and Saar, M. O. (2004). Did melting glaciers cause volcanic eruptions in eastern California? Probing the mechanics of dike formation. *J. Geophys. Res.* 109. doi:10.1029/2004JB002978

Jones, J. G. (1969)., 124. London, 197–211. doi:10.1144/gsjgs.124.1.0197Intraglacial volcanoes of the laugarvatn region, south-west Iceland—IQ. *J. Geol. Soc.*

Jones, J. G. (1970). Intraglacial volcanoes of the laugarvatn region, southwest Iceland, II. *J. Geol.* 78, 127–140. doi:10.1086/627496

Jordan, T. A., Riley, T. R., and Siddoway, C. S. (2020). The geological history and evolution of West Antarctica. *Nat. Rev. Earth Environ.* 1, 117–133. doi:10.1038/s43017-019-0013-6

Jull, M., and McKenzie, D. (1996). The effect of deglaciation on mantle melting beneath Iceland. *J. Geophys. Res.* 101, 21815–21828. doi:10.1029/96jb01308

Kano, K. (1998). A shallow-marine alkali-basalt tuff cone in the Middle Miocene jinzai formation, izumo, SW Japan. *J. Volcanol. Geotherm. Res.* 87, 173–191. doi:10.1016/s0377-0273(98)00098-5

Kokelaar, B. P. (1983a), 140. London, 939–944. doi:10.1144/gsjgs.140.6.0939The mechanism of Surtseyan volcanism*J. Geol. Soc.*

Kokelaar, P. (1986). Magma-water interactions in subaqueous and emergent basaltic. *Bull. Volcanol.* 48, 275–289. doi:10.1007/bf01081756

Kuiper, K. F., Deino, A., Hilgen, F. J., Krijgsman, W., Renne, P. R., and Wijbrans, J. R. (2008). Synchronizing rock clocks of Earth history. *Science* 320, 500–504. doi:10.1126/science.1154339

Latutrie, B., and Ross, P.-S. (2020). What lithic clasts and lithic-rich facies can tell us about diatreme processes: An example at round butte, Hopi buttes volcanic field, Navajo nation, Arizona. *J. Volcanol. Geotherm. Res.* 411, 107150. doi:10.1016/j.jvolgeores.2020.107150

Le Maitre, R. W., Streckeisen, A., Zanettin, B., and 12 authors (2002), Igneous rocks. A classification and glossary of terms. *Recommendations of the international union of geological sciences subcommission on the systematics of igneous rocks*. Cambridge: Cambridge University Press, 236.

Lee, M. J., Lee, J. I., Kim, T. H., Lee, J., and Nagao, K. (2015). Age, geochemistry and Sr-Nd-Pb isotopic compositions of alkali volcanic rocks from Mt. Melbourne and the Western Ross Sea, Antarctica. *Geosciences J.* 19, 681–695. doi:10.1007/s12303-015-0061-y

LeMasurier, W. E. (2008). Neogene extension and basin deepening in the West Antarctic rift inferred from comparisons with the East African rift and other analogs. *Geology* 36, 247–250. doi:10.1130/g24363a.1

Lescinsky, D. T., and Fink, J. H. (2000). Lava and ice interaction at stratovolcanoes—Use of characteristic features to determine past glacial extents and future volcanic hazards. *J. Geophys. Res.* 105, 23711–23726. doi:10.1029/2000jb900214

Lisiecki, L. E., and Raymo, M. E. (2005). A Pliocene-Pleistocene stack of 57 globally distributed benthic $\delta18O$ records. *Paleoceanography* 20, PA1003. doi:10.1029/2004PA001071

Long, P. E., and Wood, B. J. (1986). Structures, textures and cooling histories of Columbia River basalt flows. *Geol. Soc. Am. Bull.* 97, 1144–1155. doi:10.1130/0016-7606(1986)97<1144:stacho>2.0.co;2

Lyon, G. L. (1986). Stable isotope stratigraphy of ice cores and the age of the last eruption at Mount Melbourne, Antarctica. *N. Z. J. Geol. Geophys.* 29, 135–138. doi:10.1080/00288306.1986.10427528

Lyon, G. L., and Giggenbach, W. F. (1974). Geothermal activity in Victoria Land, Antarctica. *N. Z. J. Geol. Geophys.* 17, 511–521. doi:10.1080/00288306.1973.10421578

Maclennan, J., Jull, M., McKenzie, D., Slater, L., and Grönvold, K. (2002). The link between volcanism and deglaciation in Iceland. *Geochem. Geophys. Geosystems* 3, 1–25. doi:10.1029/2001gc000282

Martin, A. P., Cooper, A. F., Price, R. C., Kyle, P. R., and Gamble, J. A. (2021). *Erebus volcanic province: Petrology*, 55. London, Memoirs: Geological Society, 447–489.

Mee, K., Tuffen, H., and Gilbert, J. S. (2006). Snow-contact volcanic facies and their use in determining past eruptive environments at Nevados de Chillán volcano, Chile. *Bull. Volcanol.* 68, 363–376. doi:10.1007/s00445-005-0017-6

Moorhouse, B. L., and White, J. D. L. (2016). Interpreting ambiguous bedforms to distinguish subaerial base surge from subaqueous density current deposits. *Depositional Rec.* 2, 173–195. doi:10.1002/dep2.20

Mulder, T., and Alexander, J. (2001). The physical character of subaqueous sedimentary density flows and their deposits. *Sedimentology* 48, 269–299. doi:10.1046/j.1365-3091.2001.00360.x

Narcisi, B., and Petit, J. R. (2021). *Englacial tephras of east Antarctica*, 55. London, Memoirs: Geological Society, 649–664.

Nathan, S., and Schulte, F. J. (1968). Geology and petrology of the campbell–aviator divide, northern Victoria Land, Antarctica. *N. Z. J. Geol. Geophys.* 11, 940–975. doi:10.1080/00288306.1968.10420762

Niespolo, E. M., Rutte, D., Deino, A. L., and Renne, P. R. (2017). Intercalibration and age of the Alder Creek sanidine $^{40}Ar/^{39}Ar$ standard. *Quat. Geochronol.* 39, 205–213. doi:10.1016/j.quageo.2016.09.004

Ort, M. H., Lefebvre, N. S., Neal, C. A., McConnell, V. S., and Wohletz, K. H. (2018). Linking the Ukinrek 1977 maar-eruption observations to the tephra deposits: New insights into maar depositional processes. *J. Volcanol. Geotherm. Res.* 360, 36–60. doi:10.1016/j.jvolgeores.2018.07.005

Panter, K. S., Castillo, P., Krans, S., authors, 7, McIntosh, W., Valley, J. W., et al. (2018). Melt origin across a rifted continental margin: A case for subduction-related metasomatic agents in the lithospheric source of alkaline basalt, NW Ross Sea, Antarctica. *J. Petrology* 59, 517–558. doi:10.1093/petrology/egy036

Panter, K. S., Wilch, T. I., Smellie, J. L., Kyle, P. R., and McIntosh, W. C. (2021). *Marie Byrd Land and Ellsworth Land: petrology*, 55. London, Memoirs: Geological Society, 577–614.

Pedersen, G. B. M., Grosse, P., and Gudmundsson, M. T. (2020). Morphometry of glaciovolcanic edifices from Iceland: Types and evolution. *Geomorphology* 368, 107334. doi:10.1016/j.geomorph.2020.107334

Pollock, M., Edwards, B. R., Hauksdottir, S., Alcorn, R., and Bowman, L. (2014). Geochemical and lithostratigraphic constraints on the formation of pillow-dominated tindars from Undirhlíðar quarry, Reykjanes Peninsula, southwest Iceland. *Lithos* 200-201, 317–333. doi:10.1016/j.lithos.2014.04.023

Resing, J. A., Rubin, K. H., Embley, R. W., 20 authorsBaker, E. T., Dziak, R. P., et al. (2011). Active submarine eruption of boninite in the northeastern Lau Basin. *Nat. Geosci.* 4, 799–806. doi:10.1038/ngeo1275

Rhee, H. H., Lee, M. K., Seong, Y. B., Lee, J. I., Yoo, K.-C., and Yu, B. Y. (2020). Post-LGM dynamic deglaciation along the Victoria Land coast, Antarctica. *Quat. Sci. Rev.* 247, 106595. doi:10.1016/j.quascirev.2020.106595

Rocchi, S., Di Vincenzo, G., and Armienti, P. (2005). No plume, no rift magmatism in the West Antarctic rift. *Geol. Soc. Am. Special Pap.* 388, 435–447.

Rocchi, S., Di Vincenzo, G., and Ghezzo, C. (2004). The Terra Nova intrusive complex (Victoria Land, Antarctica). *Terra Antartica Rep.* 10, 1–50.

Rocchi, S., and Smellie, J. L. (2021). *Northern Victoria Land: Petrology*, 55. London, Memoirs: Geological Society, 383–413.

Rocchi, S., Storti, F., Di Vincenzo, G., and Rossetti, F. (2003). Intraplate strike-slip tectonics as an alternative to mantle plume activity for the Cenozoic rift magmatism in the Ross Sea region, Antarctica. *Geol. Soc. Lond. Spec. Publ.* 210, 145–158. doi:10.1144/gsl.sp.2003.210.01.09

Romero, J. E., Polacci, M., Watt, S., Tormey, D., Sielfeld, G., Arzilli, F., et al. (2021). Volcanic lateral collapse processes in mafic arc edifices: A review of their driving processes, types and consequences. *Front. Earth Sci.* 9, 639825. doi:10.3389/feart.2021.639825

Russell, J. K., Edwards, B. R., and Porritt, L. A. (2013). Pyroclastic passage zones in glaciovolcanic sequences. *Nat. Commun.* 4, 1788. doi:10.1038/ncomms2829

Salvini, F., Brancolini, G., Busetti, M., Storti, F., Mazzarini, F., and Coren, F. (1997). Cenozoic geodynamics of the Ross Sea region, Antarctica: Crustal extension, intraplate strike-slip faulting, and tectonic inheritance. *J. Geophys. Res.* 102, 24669–24696. doi:10.1029/97jb01643

Schmincke, H.-U., and Bednarz, U. (1990). "Pillow, sheet-flow and breccia volcanoes and volcano-tectonic cycles in the Extrusive Series of the northeastern Troodos ophiolite (Cyprus)," in *Ophiolites: Oceanic crustal analogues*. Editors J. Malpas, E. M. Moores, A. Panayiotou, and C. Xenophontos (Nicosia, Cyprus: Geological Survey Department), 185–206.

Schopka, H. H., Gudmundsson, M. T., and Tuffen, H. (2006). The formation of helgafell, southwest Iceland, a monogenetic subglacial hyaloclastite ridge: Sedimentology, hydrology and volcano-ice interaction. *Bull. Volcanol.* 152, 359–377. doi:10.1016/j.jvolgeores.2005.11.010

Self, S., Keszthelyi, L., and Thordarson, Th. (1998). The importance of pāhoehoe. *Annu. Rev. Earth Planet. Sci.* 26, 81–110. doi:10.1146/annurev.earth.26.1.81

Self, S., Thordarson, Th., Keszthelyi, L., authors, 5, Hon, K., Murphy, M. T., et al. (1996). A new model for the emplacement of Columbia River basalts as large, inflated pahoehoe lava flow fields. *Geophys. Res. Lett.* 23, 2689–2692. doi:10.1029/96gl02450

Siddoway, C. S. (2021). "The geology of West Antarctica," in *Geology of the antarctic continent*. Editor G. Kleinschmidt (Stuttgart: Gebrüder Borntraeger Verlagsbuchhandlung), 87–131.

Skilling, I. P. (1994). Evolution of an englacial volcano: Brown bluff, Antarctica. *Bull. Volcanol.* 56, 573–591. doi:10.1007/bf00302837

Skilling, I. P. (2009). Subglacial to emergent basaltic volcanism at hlöðufell, south-west Iceland: A history of ice-confinement. *J. Volcanol. Geotherm. Res.* 186, 276–289. doi:10.1016/j.jvolgeores.2009.05.023

Smellie, J. L. (2021). *Antarctic volcanism: volcanology and palaeoenvironmental overview*, 55. London, Memoirs: Geological Society, 19–42.

Smellie, J. L., and Edwards, B. E. (2016). *Glaciovolcanism on Earth & Mars. Products, processes and palaeoenvironmental significance*. Cambridge University Press, 483.

Smellie, J. L. (2018). "Glaciovolcanism – A 21st century proxy for palaeo-ice," in *Past Glacial Environments (sediments, forms and techniques)*. Editors J. Menzies and J. J. M. van der Meer 2nd edition (Amsterdam, Netherlands: Elsevier), 335–375.

Smellie, J. L. (2001). "Lithofacies architecture and construction of volcanoes erupted in englacial lakes: Icefall nunatak, mount murphy, eastern marie byrd Land, Antarctica,"in *Volcaniclastic sedimentation in lacustrine settings*. Editors J. D. L. White and N. Riggs *International Association of Sedimentologists Special Publications* (Oxford: Blackwell Science), 30, 9–34.

Smellie, J. L., and Martin, A. P. (2021). *Erebus volcanic province: Volcanology*, 55. London, Memoirs: Geological Society, 415–446.

Smellie, J. L. (2013). "Quaternary vulcanism: Glaciovolcanic landforms," in *The encyclopedia of Quaternary science*. Editor S. A. Elias 3rd edition (Amsterdam: Elsevier), Vol. 1. (In press).

Smellie, J. L., Rocchi, S., and Armienti, P. (2011a). Late Miocene volcanic sequences in northern Victoria Land, Antarctica: Products of glaciovolcanic eruptions under different thermal regimes. *Bull. Volcanol.* 73, 1–25. doi:10.1007/s00445-010-0399-y

Smellie, J. L., Rocchi, S., Gemelli, M., Di Vincenzo, G., and Armienti, P. (2011b). A thin predominantly cold-based Late Miocene East Antarctic ice sheet inferred from glaciovolcanic sequences in northern Victoria Land, Antarctica. *Palaeogeogr. Palaeoclimatol. Palaeoecol.* 307, 129–149. doi:10.1016/j.palaeo.2011.05.008

Smellie, J. L., Rocchi, S., Johnson, J. S., Di Vincenzo, G., and Schaefer, J. M. (2018). A tuff cone erupted under frozen-bed ice (northern Victoria Land, Antarctica): Linking glaciovolcanic and cosmogenic nuclide data for ice sheet reconstructions. *Bull. Volcanol.* 80, 12. doi:10.1007/s00445-017-1185-x

Smellie, J. L., and Rocchi, S. (2021). *Northern Victoria Land: Volcanology*, 55. London, Memoirs: Geological Society, 347–381.

Smellie, J. L. (2006). The relative importance of supraglacial versus subglacial meltwater escape in basaltic subglacial tuya eruptions: An important unresolved conundrum. *Earth-Science Rev.* 74, 241–268. doi:10.1016/j.earscirev.2005.09.004

Smellie, J. L., Wilch, T., and Rocchi, A. (2013). 'A'ā lava-fed deltas: A new reference tool in paleoenvironmental studies. *Geology* 41, 403–406. doi:10.1130/g33631.1

Sohn, C., and Sohn, Y. K. (2019). Distinguishing between primary and secondary volcaniclastic deposits. *Sci. Rep.* 9, 12425. doi:10.1038/s41598-019-48933-4

Sohn, Y. K., and Chough, S. K. (1992). The ilchulbong tuff cone, cheju island, South Korea: Depositional processes and evolution of an emergent, surtseyan-type tuff cone. *Sedimentology* 39, 523–544. doi:10.1111/j.1365-3091.1992.tb02135.x

Sohn, Y. K. (1996). Hydrovolcanic processes forming basaltic tuff rings and cones on Cheju Island, Korea. *Geol. Soc. Am. Bull.* 108, 1199–1211. doi:10.1130/0016-7606(1996)108<1199:hpfbtr>2.3.co;2

Sohn, Y. K., Park, K. H., and Yoon, S. H. (2008). Primary versus secondary and subaerial versus submarine hydrovolcanic deposits in the subsurface of Jeju Island, Korea. *Sedimentology* 55, 899–924. doi:10.1111/j.1365-3091.2007.00927.x

Solgevik, H., Mattsson, H. B., and Hermelin, O. (2007). Growth of an emergent tuff cone: Fragmentation and depositional processes recorded in the capelas tuff cone, são miguel, azores. *J. Volcanol. Geotherm. Res.* 159, 246–266. doi:10.1016/j.jvolgeores.2006.06.020

Storti, F., Salvini, F., Rossetti, F., and Phipps Morgan, J. (2007). Intraplate termination of transform faulting within the Antarctic continent. *Earth Planet. Sci. Lett.* 260, 115–126. doi:10.1016/j.epsl.2007.05.020

Takada, A. (1994). The influence of regional stress and magmatic input on styles of monogenetic and polygenetic volcanism. *J. Geophys. Res.* 99, 13563–13573. doi:10.1029/94jb00494

Valentine, G. A., Graettinger, A. H., and Sonder, I. (2014). Explosion depths for phreatomagmatic eruptions. *Geophys. Res. Lett.* 41, 3045–3051. doi:10.1002/2014gl060096

Vespermann, D., and Schmincke, H.-U. (2000). "Scoria cones and tuff rings," in *Encyclopedia of volcanoes*. Editor H. Sigurdsson (San Diego: Academic Press), 683–694.

Vincenzo, G. D., and Rocchi, S. (1999). Origin and interaction of mafic and felsic magmas in an evolving late orogenic setting: The early paleozoic Terra Nova intrusive complex, Antarctica. *Contributions Mineralogy Petrology* 137, 15–35. doi:10.1007/s004100050579

Walker, G. P. L. (1992). Morphometric study of pillow-size spectrum among pillow lavas. *Bull. Volcanol.* 54, 459–474. doi:10.1007/bf00301392

W. E. LeMasurier and J. W. Thomson (Editors) (1990). "Volcanoes of the Antarctic plate and southern oceans,", 48, 487.*Am. Geophys. Union, Antarct. Res. Ser.*

Watt, S. F. L., Pyle, D. M., and Mather, T. A. (2013). The volcanic response to deglaciation: Evidence from glaciated arcs and a reassessment of global eruption records. *Earth-Science Rev.* 122, 77–102. doi:10.1016/j.earscirev.2013.03.007

White, J. D. L., and Houghton, B. F. (2006). Primary volcaniclastic rocks. *Geology* 34, 677–680. doi:10.1130/g22346.1

White, J. D. L. (1996). Pre-emergent construction of a lacustrine basaltic volcano, Pahvant Butte, Utah (USA). *Bull. Volcanol.* 58, 249–262. doi:10.1007/s004450050138

White, J. D. L., and Ross, P. S. (2011). Maar-diatreme volcanoes: A review. *J. Volcanol. Geotherm. Res.* 201, 1–29. doi:10.1016/j.jvolgeores.2011.01.010

White, J. D. L., Smellie, J. L., and Clague, D. (2003). *Introduction: A deductive outline and topical overview of subaqueous explosive volcanism*, 140. American Geophysical Union Geophysical Monographs, 1–23.

White, J. D. L. (2000). Subaqueous eruption-fed density currents and their deposits. *Precambrian Res.* 101, 87–109. doi:10.1016/s0301-9268(99)00096-0

Wilch, T. I., McIntosh, W. C., and Panter, K. S. (2021). Marie Byrd Land and Ellsworth Land: volcanology. *Geological Society, London, Memoirs*, 55, 515–576.

Wilson, A. M., and Russell, J. K. (2020). Glacial pumping of a magma-charged lithosphere: A model for glaciovolcanic causality in magmatic arcs. *Earth Planet. Sci. Lett.* 548, 116500. doi:10.1016/j.epsl.2020.116500

Wilson, L., Smellie, J. L., and Head, J. W. (2013). "Volcano-ice interaction," in *Modeling of volcanic processes: The physics and mathematics of volcanism*. Editors S. A. Fagents, T. K. P. Gregg, and R. M. C. Lopes (Cambridge: Cambridge University Press), 275–299.

Witham, A. G., and Sparks, R. S. J. (1986). Pumice. *Bull. Volcanol.* 48, 209–223. doi:10.1007/bf01087675

Wohletz, K. H., and Sheridan, M. F. (1983). Hydrovolcanic explosions II. Evolution of basaltic tuff rings and tuff cones. *Am. J. Sci.* 283, 385–413. doi:10.2475/ajs.283.5.385

Wohletz, K. H. (2003). *Water/magma interaction: Physical considerations for the deep submarine environment*, 140. American Geophysical Union Geophysical Monographs, 25–49.

Wörner, G., Niephaus, H., Hertogen, J., and Viereck, L. (1989). The Mt. Melbourne volcanic field (Victoria Land, Antarctica), II. Geochemistry and magma Genesis. *Geol. Jahrb.* E38, 395–433.

Wörner, G., and Orsi, G. (1990). Volcanic geology of Edmonson point, Mt. Melbourne volcanic field, north Victoria Land, Antarctica. *Polarforschung*. Bremerhaven: Alfred Wegener Institut 60, 84–86.

Wörner, G., and Viereck, L. (1990). *Mount Melbourne*, 48. American Geophysical Union, Antarctic Research Series, 72–78.

Wörner, G., and Viereck, L. (1987). Subglacial to emergent volcanism at shield nunatak, Mt. Melbourne volcanic field, Antarctica. *Polarforschung* 57, 27–41.

Wörner, G., and Viereck, L. (1989). The Mt Melbourne volcanic field (Victoria Land, Antarctica). I. Field observations. *Geol. Jahrb.* E38, 369–393.

Zimanowski, B., and Büttner, R. (2003). *Phreatomagmatic explosions in subaqueous volcanism*, 140. American Geophysical Union Geophysical Monographs, 51–60.